



**Southeast Environmental Research Center**  
FLORIDA INTERNATIONAL UNIVERSITY

**Annual Report: ecosystem dynamics in the White Zone: history,  
drivers, and restoration implications**

**Task Agreement # P15AC01625**  
**Cooperative Agreement # H5000-10-5040**

Period: October 4, 2015 to October 3, 2016

**Submitted to:**

**David Rudnick**

South Florida Natural Resources Center  
Everglades and Dry Tortugas National Parks  
950 N. Krome Ave., Homestead, FL 33030-4443  
Tel. 305-338-3508, Fax. 305-224-4147  
Email: David\_Rudnick@nps.gov

**Mike Ross, Jack Meeder, Anna Wachnicka, Len Scinto, Jay Sah,  
Susana Stoffella, Danielle Ogurcak, Rosario Vidales, and Sean Charles**  
Southeast Environmental Research Center  
Florida International University, Miami FL 33199

2016

## Table of Contents

Introduction – Project history and purpose ( <b>Mike Ross</b> )	3
Study Design and Progress during 2015-2016 ( <b>Mike Ross</b> )	3
Results	4
1. Marsh vegetation pattern, dynamics, and function	
1.1. Marsh vegetation change in the C111 basin over last two decades based on resampled plots ( <b>Susana Stoffella</b> )	4
1.2. Marsh vegetation change in the C111 basin over last two decades based on LANDSAT imagery ( <b>Danielle Ogurcak</b> )	7
1.3. Change in vegetation in the L-31E project area over last three decades based on resampled plots and LANDSAT imagery ( <b>Rosario Vidales and Danielle Ogurcak</b> )	13
2. Environmental and paleo-indicators	
2.1. Diatom patterns in surface sediments ( <b>Anna Wachnicka</b> )	22
2.2. Mollusk composition in sediment profiles ( <b>Jack Meeder</b> )	30
3. Soils	
3.1. Root biomass ( <b>Sean Charles</b> )	43
3.2. Soils ( <b>Mike Ross</b> )	47
Other products ( <b>Mike Ross</b> )	48
Plans for 2016-17 ( <b>Mike Ross</b> )	48
Literature	48

## INTRODUCTION

Sea level rise (SLR) is destined to be a critical variable in the future of the Everglades, but until recently, its potential impacts were notably absent from restoration planning considerations. Like the proverbial elephant sitting in the corner, SLR could not be ignored indefinitely, and Everglades managers and planners are now working hard to incorporate it into the planning process. However, this will not be an easy task. For one thing, the integration of SLR into planning will require a fuller and more detailed vision of how coastal ecosystems will respond to concurrent changes in sea-level and fresh-water delivery, especially when changes in the former are expected to accelerate far beyond the current rate. Development of such a model might start with relationships gained from spatially explicit information on the structure, function, and recent dynamics of wetlands exposed to known rates of SLR and receiving known volumes of fresh water delivery; from there, it may be possible to contemplate future scenarios that include a more rapidly rising sea with more confidence.

In the marshes and swamps the coastal plain south and east of the Miami Rock Ridge, an ecological sampling network is in place that can generate some of the data needed to populate the needed models discussed above. In 1993-94, an FIU research group lead by Mike Ross and Jack Meeder undertook a study of the Southeast Saline Everglades, a landscape that was named and described four decades earlier by Frank Egler, one of the giants of 20<sup>th</sup> Century vegetation science (Egler 1952). The FIU study (Meeder et al. 1996) demonstrated that both SLR and fresh-water discharge exerted important controls on plant and mollusk community dynamics, as well as on the relative proportions of organic and carbonate material in coastal soils. Ecological changes consistent with salt water intrusion were greatest in wetlands that had long been cut off from upstream fresh-water sources, and least in wetlands still receiving fresh-water discharge. The Meeder et al. (1996) report and subsequent papers (Ross et al. 2000; Ross et al. 2002) demonstrated that the interior border of the white zone – a zone of low productivity, previously described by Egler, in which a light-colored marl substrate is exposed by the low vegetation cover - is a broad but effective marker of coastal transgression, and the composition of plant, mollusk, and diatom assemblages along the gradient are sensitive indicators of local conditions. Tree islands scattered across this landscape appeared to be somewhat more resistant to salt water influence than the surrounding marsh communities, but nevertheless are distributed in a similar zonal arrangement relative to the coast (Ross et al. 2013). In the fall of 2015, the FIU research team began a re-survey of the Southeast Saline Everglades, intending to (1) document any changes that may have occurred during the past two decades, and (2) interpret such changes from the perspective that twenty years of advances in coastal wetland science might provide. This Report describes progress made during Year 1 of a 3-year research effort.

## STUDY DESIGN

In 1993-94, our group sampled vegetation and soils at 56 sites in the Southeast Saline Everglades (SESE), ranging from Taylor Slough on the west to Turkey Point on the east (Meeder et al. 1996). Sample locations were distributed along seven transects perpendicular to the Florida Bay or Biscayne Bay coastline. Vegetation cover ranged from pure mangrove swamp near the coast to homogeneous sawgrass marsh in the interior. Many of the sites had been sampled previously by other Everglades scientists, or hosted active water level recorders.

In the current project, which continues through 2018, our intention is to resample a subset of 31 of the original sites, while adding 11 sites in coastal marshes west of Taylor Slough, and 8 sites north of Barnes Sound, including four in the L-31E Pilot Project site (**Figure 1**). Our design calls for sampling in the marsh (or swamp) matrix during the dry season (January – May), and in the closest well-developed tree island to the marsh plot center during the wet season (October – December).

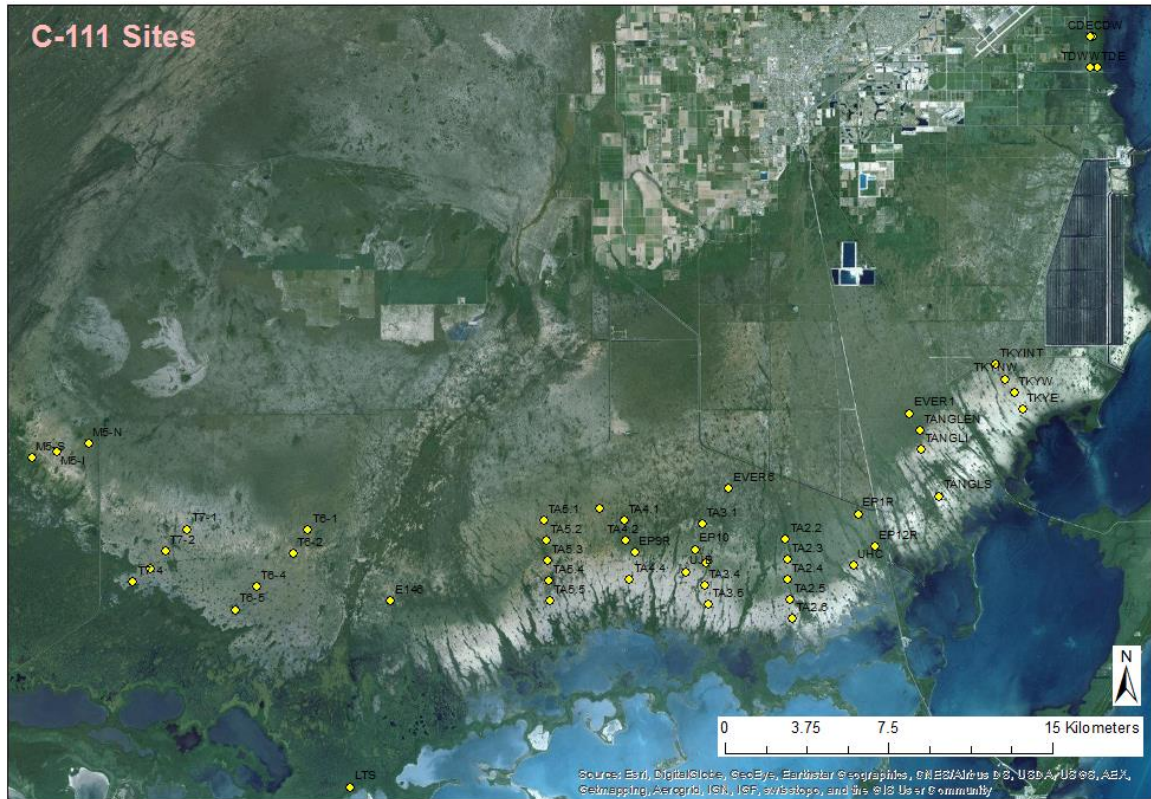


**Figure 1:** Map showing the location of sites proposed for vegetation sampling.

This year, we completed marsh vegetation and soil sampling at 24 of the 50 intended sites, plus two additional Fringe forest sites along the Biscayne Bay coastline in the Pilot Project area. Below, we describe some preliminary results from our surveys of (1) marsh vegetation, (2) environmental indicators, including diatoms and mollusk indicators of paleosalinity, and (3) soil and water characteristics.

## RESULTS

### 1. Marsh vegetation pattern, dynamics, and function

#### 1.1. Marsh vegetation change in the C111 basin over last two decades based on resampled plots

In the marsh, all vascular plant species were identified in 30 1 m<sup>2</sup> subplots distributed evenly along a 360<sup>0</sup> arc at 50 m distance from the plot center, and water and soil depth were also determined. At the plot center, porewater was collected, along with a short soil core (~40 cm) for assessment

of nutrient availability in different strata within the profile. A second, deeper core (to bedrock or 1.4 m) was also extracted for paleoecological study. Three sets of red mangrove leaves (if present) were collected for determination of carbon, nitrogen, and phosphorus content, as well as carbon isotope ratio. Finally, a sample from the upper 2 cm of the soil was collected and returned to the lab for analysis of diatom composition.

Of the 24 sites where marsh sampling was completed during January and March 2016, fourteen had been sampled in 1994-96 with similar methods to those described above (**Table 1.1.1**). Several locations, especially TKYW, needed to be shifted slightly in order to accommodate helicopter access, but in general were within 100 m or so of the original location.

<b>Table 1.1.1:</b> Sites sampled in 1994-96 and 2016.			
1990s Site #	Sites sampled in 1996	2016 Site #	Sites sampled in 2016
		1	CDE
		2	CDW
1	EP12R	3	EP12R
2	EVER1	4	EVER1
		5	M5-N
3	TA2.2	6	TA2.2
4	TA2.3	7	TA2.3
5	TA2.4	8	TA2.4
6	TA2.5	9	TA2.5
7	TA2.6	10	TA2.6
8	TA3.3	11	TA3.3
9	TA3.4	12	TA3.4
10	TA3.5	13	TA3.5
		14	TANGLN
		15	TANGLI
		16	TANGLS
		17	TDE
		18	TDWW
11	TKYE	19	TKYE
12	TKYINT	20	TKYINT
13	TKYN		
		21	TKYNW
		22	TKYW
14	UHC	23	UHC
15	UJB	24	UJB

Multivariate techniques, including non-metric multidimensional scaling (NMS) ordination (McCune and Grace 2002) were used to describe vegetation:environment relationships. The analyses were applied to all 39 site x time combinations listed in **Table 1.1.1**, allowing us to examine temporal shifts in species composition along a distance-to-coast gradient. Species frequency was calculated for each site, and then relativized to the maximum frequency for the species in any plot. Species present only in one site were excluded from the analysis, leaving 16 species present in multiple sites. The relationship between species composition and distance to

coast was examined using Mantel test (McCune and Grace 2002). The ordination axes were firmly rotated so that axis 1 was aligned with distance to coast and the second axis was orthogonal to the first axis on the ordination plane defined by the rotated axis 1 and 2. In the NMS ordination space, the direction of any shift in species composition over the sampling period was indicated by arrows connecting 1990s and 2016 positions for the same site. Analysis of similarity (ANOSIM) (Clarke et al 2005) was used to examine the significance of temporal differences in species composition across these 15 sites. Also, paired t tests were used to test for difference in matching site scores on axis 1 between 1990s and 2016.

Variation in vegetation composition among all sites over the sampling period (1996-2016) was adequately summarized by a three dimensional NMS ordination (Stress = 0.11). The analysis (**Figure 1.1.1**) indicated that marsh vegetation was primarily arranged along a gradient of distance to the coast; distance to coast was significantly correlated to species composition (Mantel test 999 permutations,  $r=0.25$ ,  $p<0.05$ ). Inland marsh sites, distributed on the right side of Axis 1, are characterized by sawgrass (*C. jamaicense*) or spikerush (*Eleocharis cellulosa*). The negative side of Axis 1 is occupied by coastal sites dominated by halophytes like saltgrass (*Distichlis spicata*), seapurslane (*Sesuvium portulacastrum*) and several mangrove species: white mangrove (*Laguncularia racemosa*), black mangrove (*Avicennia germinans*) and buttonwood (*Conocarpus erectus*). Present at all but one site-time combination, red mangrove (*Rhizophora mangle*) occupies a position near the center of the ordination.

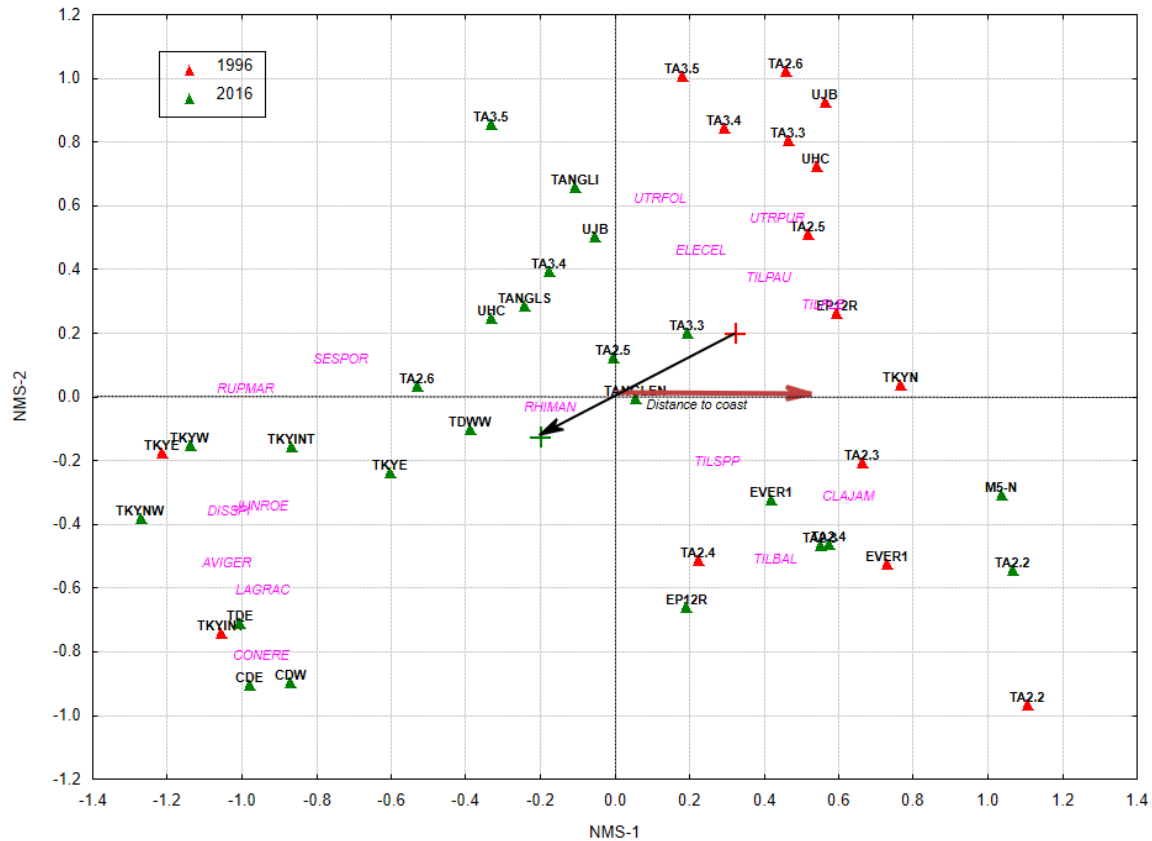


**Figure 1.1.1:** Non-metric Multidimensional Scaling (NMS) Ordination Axis-1 and 2.

1994-96 samples tend to be located on the negative side of axis 1 while those sampled in 2016 are on the opposite side. This suggests the vegetation change that took place over the intervening twenty years – a shift in species assemblages toward one more characteristic of coastal locations. Species composition differed significantly between sampling years across all site-time combinations (ANOSIM; 999 permutations,  $R = 0.204$ ,  $p\text{-value} < 0.05$ ). A t-test comparing scores at common sites sampled in 1996 and 2016 was also significant ( $t=2.35$ ,  $df=13$ ,  $p\text{-value}<0.05$ ).

## **1.2. Marsh vegetation change in the C111 basin over last two decades based on LANDSAT imagery**

Using the 1993/1994 study of vegetation sampling in the SESE as a baseline, we (a) assessed changes in vegetation over two decades using field sampling techniques and (b) investigated changes in a subset of the larger SESE using the entirety of the Landsat satellite image record 1984-2016 (30+ years). The purpose was to quantify changes in composition that should be associated with mangrove encroachment, white zone expansion, and sawgrass recession. The vegetation sampling was conducted to capture change at the start and end points of this time period, while the remote-sensing analysis was intended to track changes associated with salt water intrusion punctuated by disturbance from freeze events and hurricane storm surge.

The study area for the remote sensing work encompassed a 103 km<sup>2</sup> area which extended east-west 10.5 km from US 1 (W 80.453) to ~1 km from the coast (W 80.348), and extended south 9.8 km from the boundary of Turkey Point cooling canals (N 25.356) to Barnes and Card Sounds (N 25.268) (**Figure 1.2.1**) The area included vegetation zones along the gradient of freshwater sawgrass marsh into white zone and dwarf mangrove to the coast of Florida Bay. Within the study boundary are located four vegetation sampling sites which were sampled during both 1990s and 2016 sampling events (TKYE, TKYINT, EP12R, and EVER1). This subset of the larger C111 basin was selected to investigate the ability of remote sensing methods to detect effects of both disturbance and long-term change using moderate-resolution satellite data.

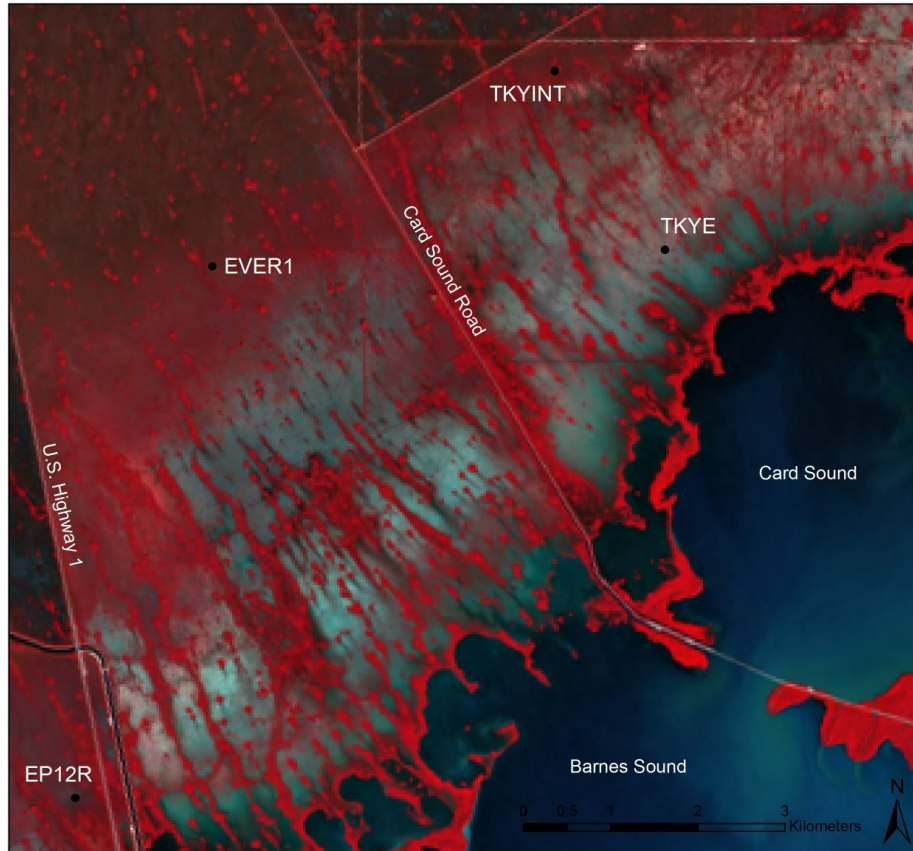


**Figure 1.2.1:** Portion of C-111 basin included in remote sensing analysis. Vegetation sampling plots are indicated by black points having a radius of 50m. Base image is Landsat 8 from January 24<sup>th</sup>, 2016 displaying the combination of NIR, red, and green bands. Brightest red areas correspond to areas of dense mangrove vegetation, while the brick red of the northwest corner is primarily sawgrass, and the white and light blue area is flooded, sparsely-vegetated white zone.

The entire temporal sequence (1984 – 2016) of Landsat spectral reflectance, including Landsat 5 TM, Landsat 7 etm+, and Landsat OLI, was obtained from the USGS (<http://earthexplorer.usgs.gov/>). The number of images available for each year of the study ranged from a minimum of less than 10 to greater than 40 in 2015 (2016 only included the scenes from the first couple months of the year) (**Figure 1.2.2**). Spectral reflectance products were derived from images which had been atmospherically corrected using the LEDAPS (Masek et al., 2006). Using the bfastSpatial package in R (Verbesselt et al. 2012), we investigated the ability of several vegetation indices to explain temporal changes in vegetation over the time period. The bfastmonitor function fits a harmonic model to data designated as falling within a stable history period of 6 years (1984-1989), and compares the model to the actual data within a defined monitoring period (1990-2016) to determine the timing of magnitude of breaks from the model (DeVries et al. 2015). Magnitude is computed as the median residual between expected values based on the stable history period and observed values throughout the monitoring period. The output generated is a spatially-explicit raster displaying magnitude of change from the stable history period for each vegetation index tested over the monitoring period. We use a threshold of 0.1 to report changes in magnitude (vegetation index values range from -1 to 1) to eliminate the effect of changes due to seasonality, etc. Another function within the package, bfmPixel, plots time series graphs of the data compared to the fitted model at specified pixel locations. We use the

sample location, TKYINT, as an example to compare the ability of several vegetation indices to track changes in vegetation at a site. As the composition of TKYINT changed over the study period (**Figure 1.2.3**) from a primarily freshwater marsh-dominated assemblage to one dominated by mangroves, it serves as evidence of continued landward migration of the white zone.

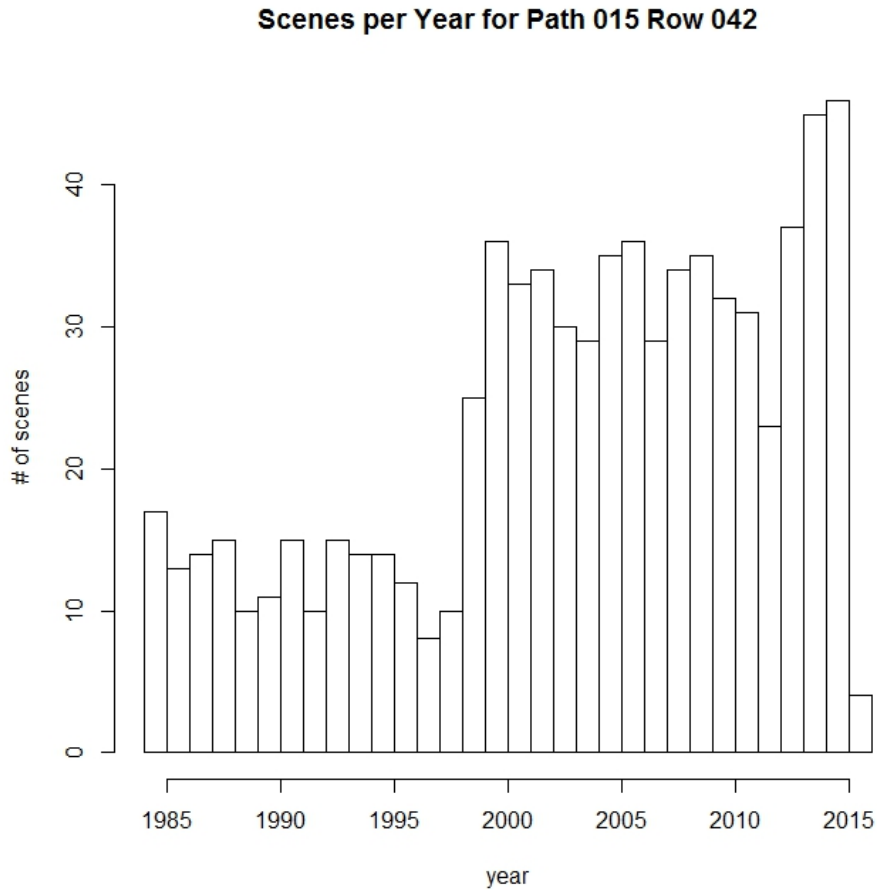


**Figure 1.2.2:** Number of Landsat images available in each year for Path 015 Row 042.

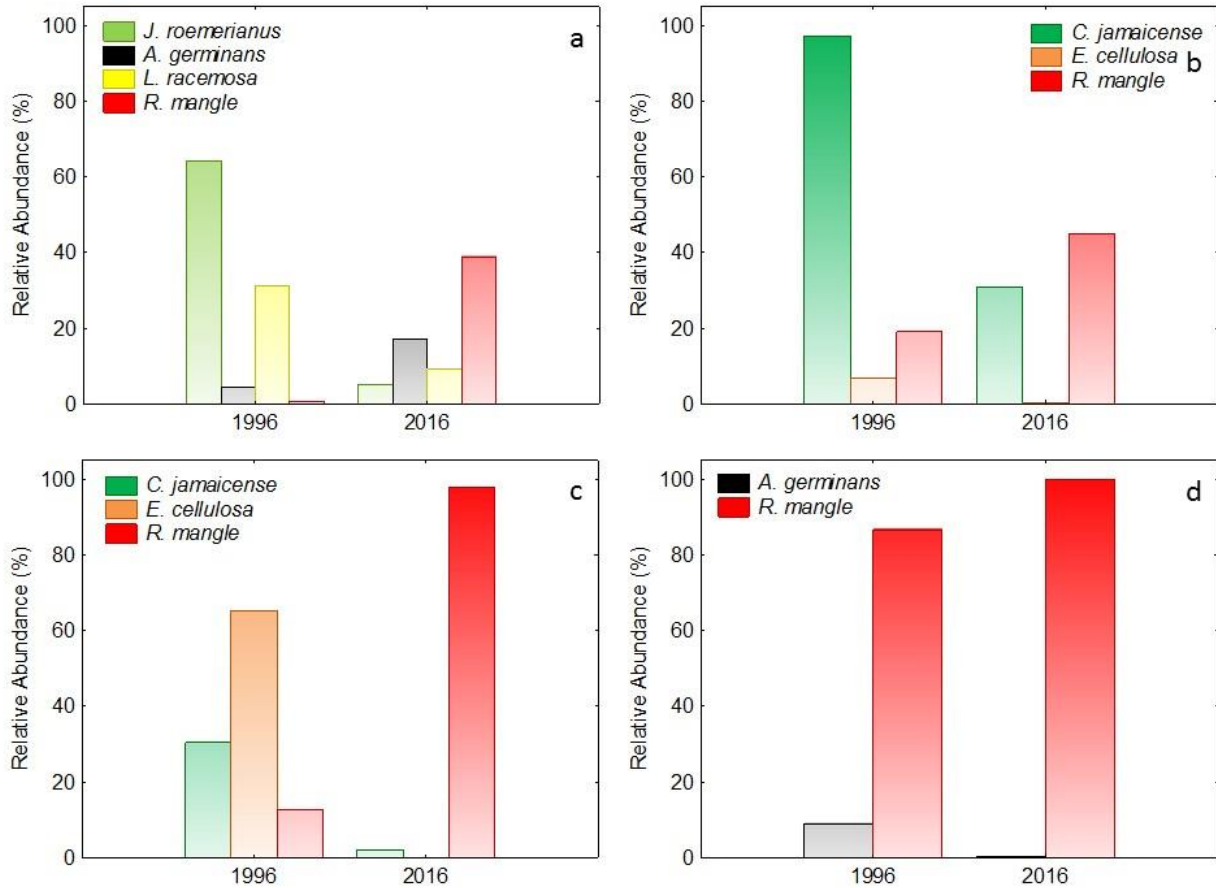


**Figure 1.2.3.** Relative abundance of dominant plant species in 1996 and 2016 at sample sites a) TKYINT, b) EVER1, c) EP12R, and d) TKYE.

For TKYINT, the fit of the NDVI data to the stable history using a harmonic model of order 3 resulted in an  $R^2 = 0.56$  (**Figure 1.2.4a**). For NDMI, the relationship was slightly stronger ( $R^2 = 0.67$ , **Figure 1.2.4b**). However, the large magnitude of annual fluctuation of NDMI suggests a large effect of changing water conditions on the reflectance of each pixel. Each vegetation index has varying sensitivity to background surface that shows through the vegetation and band 5 in NDMI is sensitive to water both in vegetation and on the ground. VI values below 0.2 likely indicate standing water. Since NDVI appeared to be less sensitive to changing ground conditions, we only show the results of bfastMonitor for NDVI. Future work will need to incorporate a spatio-temporally explicit model of water levels throughout the study area to account for the effects of water on surface reflectance.

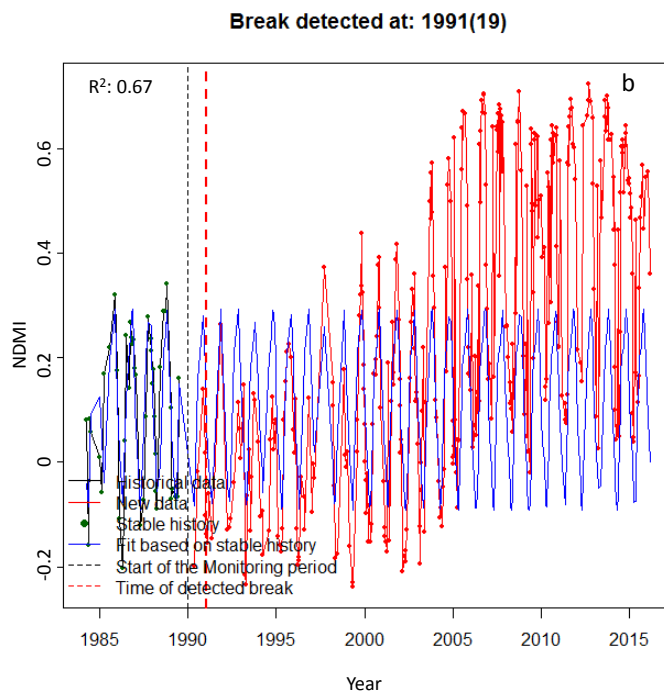
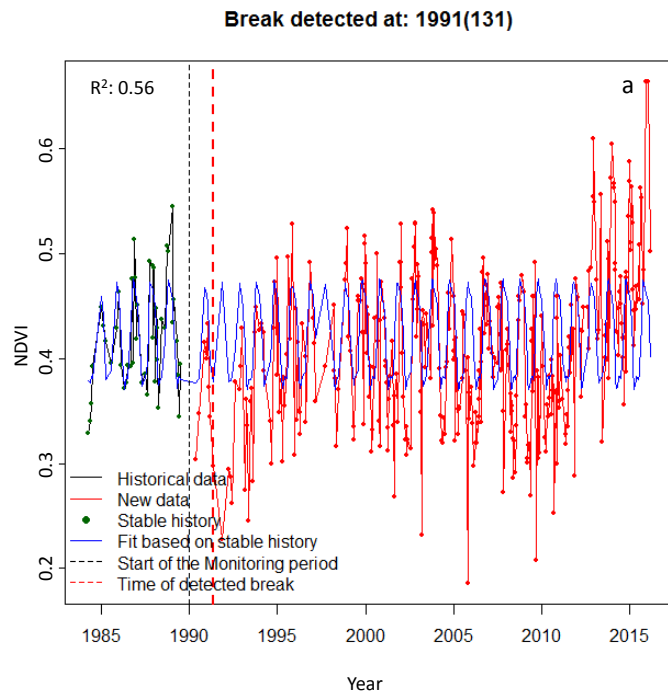


**Figure 1.2.4.** Time series of a) NDVI and b) NDMI at the TKYINT sample location with the first breakpoint detected on May 11, 1991 for NDVI and January 19, 1991 for NDMI. Series generated from the bfmPixel function in bfastSpatial package.

For both indices, a breakpoint from the stable history was detected in early 1991 (**Figure 1.2.4a and b**). This coincides with timing of a severe freeze event on December 25, 1989, which may have damaged the mangrove component at TKYINT as it did further north in the L31E basin (Zhang et al. 2016). This would put the peak of mortality from the freeze event at 1 to 1.4 years after the event suggesting that mortality was delayed for a year or more. The trend of increasing reflectance in the past several years can likely be attributed to an increase in mangrove leaf area as mangrove expands into previously freshwater-dominated wetlands; dense areas of mangroves have higher vegetation index values compared to wetland grasses/sedges.

The magnitude increase map primarily indicates increases in NDVI at locations coincident with fringing mangrove along Barnes and Card Sounds (**Figure 1.2.5**). Increase in NDVI are also present at a few locations along the C-111 canal and within the C-111 basin occupied by denser mangroves associated with inlets (**Figure 1.2.5**). The largest decreases over the time period are associated with interior areas of the current extent of the white zone (**Figure 1.2.6**). It is clear as well that greatest landward movement of the white zone occurs in the Model Lands area, east of Card Sound Road.

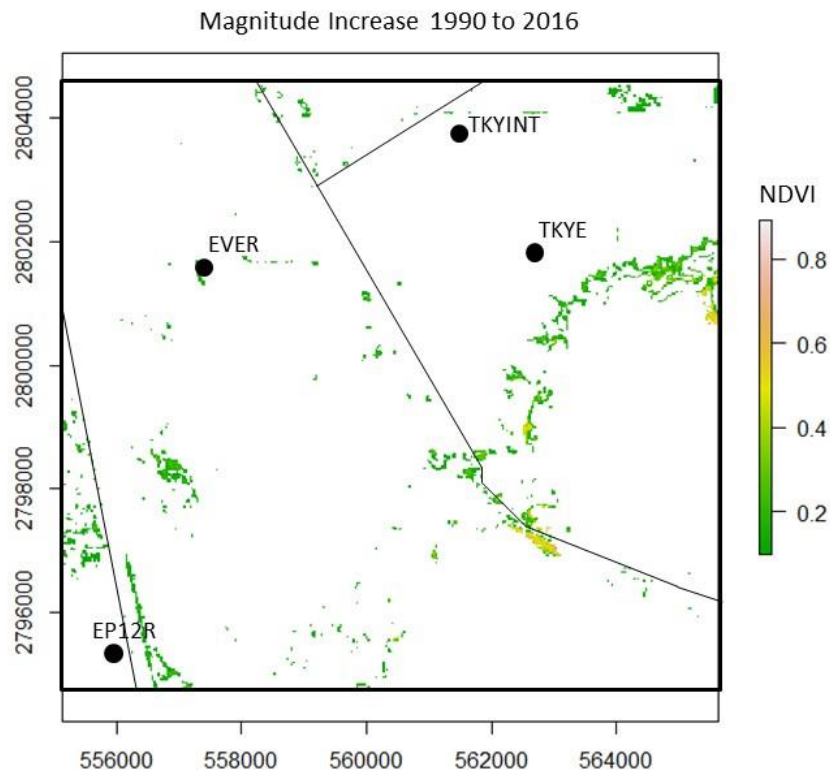


**Figure 1.2.5:** Magnitude of NDVI increase (threshold greater than 0.1) over the time period 1990 to 2016.

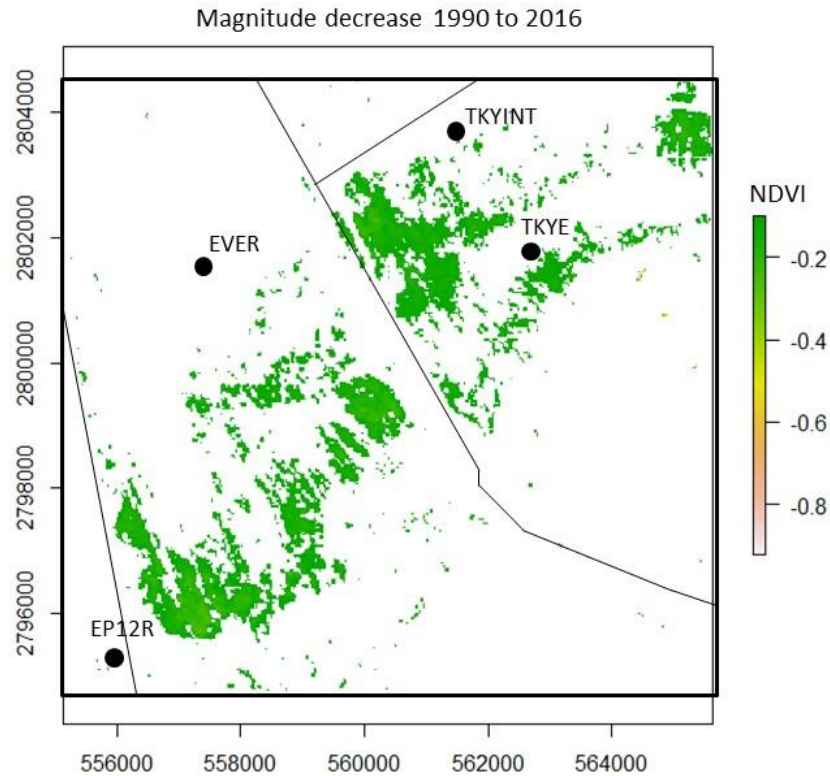


**Figure 1.2.6:** Magnitude of NDVI decrease (threshold greater than 0.1) over the time period 1990 to 2016.

### **1.3. Change in vegetation in the L-31E project area over last three decades based on resampled plots and LANDSAT imagery**

After Hurricane Andrew in 1992, study plots were established in both dwarf and fringe mangrove east of the L31E canal to document post-hurricane re-establishment of the forest. A detailed assessment of forest biomass was conducted yearly from 1994 to 2001. The goal for this portion of the project in year 1 was to resample the vegetation of these plots, assess compositional and structural change in the plots during 2001-2016, and assess the ability of the normalized difference vegetation index (NDVI), calculated from Landsat spectral reflectance values, to capture changes in forest biomass. The existence of a relationship between biomass and vegetation indices could extend the study of forest recovery from disturbance to a wider spatial area within both forest types.

The study area coincided with that of the pilot L31E study area which is located to the east of the L31E canal, and bounded on the south by the Mowry Canal (C-103) and to the north by the Military Canal (**Figure 1.3.1**). Throughout this area, the mangrove swamp consisted of a zone of Fringe forest adjacent to the coast, and Dwarf forest closer to the L31E canal. The area was further divided into 5 hydrologically independent units which were separated by drainage ditches. Two blocks were selected for monitoring: a Treatment block that received freshwater diversion from

the L-31E beginning in 1996, and a Control block, which did not. During April-July 1995, a total of 15 rectangular plots were established and censused in the two blocks. Four plots were established in the Treatment Fringe, Control Fringe and Treatment Dwarf forests, and three were established in the Control Dwarf forest. The plots were rectangular in shape, with widths of 0.5 meters and lengths varying from 3 to 10 meters (in order to establish an initial monitoring population of at least 100 individuals, if possible). All mangrove stems within these plots were tagged in April 1995, less than three years after Hurricane Andrew passed directly over the site with winds that exceeded 150 mph. The location of each stem within the plot was recorded, and height, stem diameter, and crown dimensions were measured. During the fall of 1995, and annually thereafter through 2002, the tagged individuals were re-censused as before, and newly encountered, lignified individuals that had produced a minimum of two sets of leaves were labeled with an aluminum tag and added to the database. Using allometric equations developed from mangrove stems elsewhere in the study area (Ross et al. 2001, Smith and Whelan 2006), biomass was estimated for each census period. In the Spring of 2016, these 15 plots were resampled as before, and biomass was estimated anew.

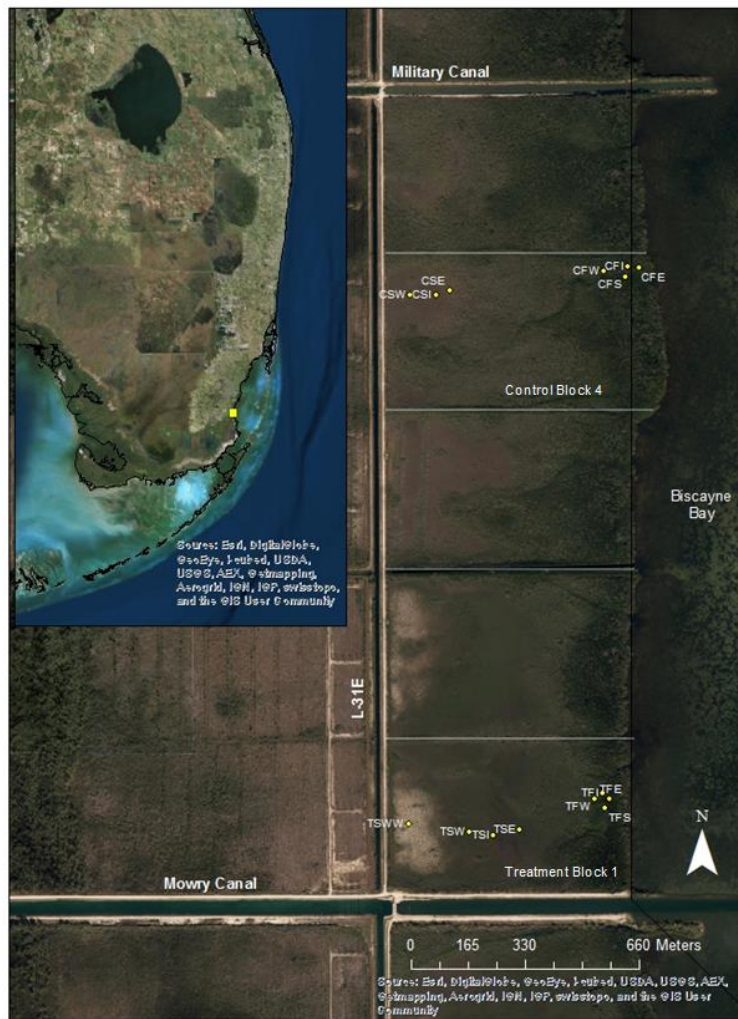


**Figure 1.3.1:** Map of the 15 mangrove census plots within the L-31E project area. Within the five blocks, the Block 1 and 4 are the Treatment and Control block respectively. The Treatment block has four dwarf mangrove scrub plots and four fringe plots, while the Control block has three scrub plots and four fringe plots.

In the dwarf mangrove plots, observations were made of species, height to base of crown (CRWNHT), total height(TOTHT), diameter at 30 cm (D<sub>30</sub>), crown length (CRWNL), and crown width (CRWNW) of each individual rooted within. To calculate dry above-ground biomass in the dwarf mangrove forest plots, we used species-specific biomass regression equations developed for *R. mangle*, *A. germinans*, and *L. racemosa* in the dwarf mangrove growth habit in the Everglades (Ross, et al., 2001).

**Table 1.3.1** Species-specific allometric equations for total dry above-ground biomass (TOTWT) in grams (Ross et al. 2001) for dwarf mangroves up to 6 meters in height within the L-31E study area. D= Diameter taken at 30 cm, CRWNV= Crown Volume or CRWNL×CRWNW×CRWNDepth (Ross et al. 2001).

Species	Equation (Ross et al. 2001)
<i>A. germinans</i>	$Ln(TOTWT) = 2.134 + (0.895 \cdot Ln(D^2)) + (0.184 \cdot Ln(CRWNV))$
<i>L. racemosa</i>	$Ln(TOTWT) = 1.095 + (0.659 \cdot Ln(D^2)) + (0.304 \cdot Ln(CRWNV))$
<i>R. mangle</i>	$Ln(TOTWT) = 2.528 + (1.129 \cdot Ln(D^2)) + (0.156 \cdot Ln(CRWNV))$

The equations use the variables: D= diameter (cm) at 30 cm, and CRWNV=crown width×crown length×crown depth (in cm) to calculate total dry above-ground biomass (TOTWT) (Ross, et al.,2001). Seedlings smaller than 40 cm height were assigned a constant weight: *R. mangle*=3.41 g, *A. germinans*= 1.3 g, *L. racemosa*= 1.61 g (Ross, et al. 2001).

No allometric equation has been previously developed for *C. erectus* of dwarf or normal growth habit. However, Castaneda-Moya et al. (2013) used the Smith and Whelan (2006) allometric relation equation of *L. racemosa* (developed with *L. racemosa* of DBH ranging from 0.7-21.5 cm) to calculate *C. erectus* above-ground biomass due to the similar growth habit of the two species. To parallel this work in the dwarf forest, we opted to use the Ross, et al. (2001) allometric relation equation developed for dwarf *L. racemosa* to calculate the dry biomass of stems of *C. erectus* present within the dwarf plots.

In the Fringe plots, observations again included species and diameter. Due to the difficulty of directly measuring tree heights in the fringe forest plots, tree heights were calculated using a clinometer and laser rangefinder: the angle to the top of the tree was obtained with the clinometer, the observer’s horizontal distance from the target tree was measured with a laser rangefinder, and the distance from the clinometer to the ground was measured manually. The total tree height was calculated by multiplying the tangent of the angle to the tree top by the distance from observer to the tree and adding the distance of the clinometer (at eye level) to the ground.

$$Tree\ Height = (Distance\ to\ ground) + (Distance\ to\ tree * \tan(angle\ to\ tree\ top))$$

To calculate above-ground biomass for the fringe plots, the Smith and Whelan (2006) allometric equation for the *R. mangle*, *A. germinans*, and *L. racemosa* mangroves and corresponding regression parameters were used. Aboveground biomass (kg) of fringe mangroves was calculated for *R. mangle*, *A. germinans*, and *L. racemosa*, according to the functional form below (see also Table 1.3.2):

$$\log_{10}y = a \log_{10}(DBH) + b \quad (\text{Smith and Whelan, 2006})$$

**Table 1.3.2** Regression parameters for use in the Smith and Whelan (2006) allometric equation ( $\log_{10}y = a \log_{10}(DBH) + b$ ) for total dry above-ground biomass,  $y$  (kg), specifically for the following mangrove DBH ranges: *Avicennia* 0.7-21.5 cm, *Laguncularia* 0.5-18.0 cm, and *Rhizophora* 0.5-20.0 cm (Smith and Whelan, 2006). The formula and regression parameters for *Laguncularia* were used for *C. erectus*, as per Castaneda-Moya et al. (2013).

Species	Regression Parameters		
	$a$	$b$	$R^2$
<i>Avicennia</i>	1.934	-0.395	0.951
<i>Laguncularia</i>	1.930	-0.441	0.977
<i>Rhizophora</i>	1.731	-0.112	0.937

Within the fringe block, two *R. mangle* shorter than breast height did not fall within the DBH range limits of the Smith and Whelan (2006) allometric equation; dry aboveground biomass value was assigned using the Ross, et al. (2001) *R. mangle* seedling constant. Fringe seedling biomass was estimated using the aforementioned Ross, et al. (2001) species constants. For two multi-stemmed *R. mangle* in the TFI and CFW plots, dry biomass was calculated for each stem separately using the Smith and Whelan (2006).

Density per hectare of mangrove stems in Treatment and Control Blocks is illustrated by size class for the 1996, 2001 and 2016 survey years of the Fringe and Dwarf forest (**Figure 1.3.2, 1.3.3**). Throughout the censuses, mangrove density per hectare remained highest in the lower canopy dwarf plots than in fringe plots. Through 2016, mangrove density in the Control Dwarf (CD) plots remained above that of the Treatment Dwarf plots (TD). Between 1996 and 2001, density of the Dwarf forests plots increased, but decreased by 2016. In the same time period, Fringe forest continuously decreased in density.

Composition of the CD plots in 1996 was dominated by *R. mangle* and *L. racemosa* up to 100 cm in height. *L. racemosa* of seedlings (1-19 cm) were increasingly present throughout the surveys, and by 2001, *L. racemosa* was dominant over *R. mangle* in the 20-39 cm size class as well. Over the same period, *R. mangle*, became more abundant in the 60-79 cm and 80-99 cm size classes. *C. erectus*, completely absent in CD plots in 1996, was present in the 60-79 cm size class by 2001. In 2016, *C. erectus* was the only species present from 100-199 cm in height, and composed an increasing proportion of individuals in the range of 40-199 cm. There was a decrease in *R. mangle* density, and an increase in the dominance of *L. racemosa* among individuals 1-79 cm. Overall, CD plots exhibited growth of *R. mangle* individuals, which later thinned out and became dominated by increasing numbers of *L. racemosa*. Change in composition was not as great in the TD plots, which was dominated by *R. mangle* and *L. racemosa*. By 2016, the overall plot density decreased, with many *R. mangle* growing into the 80-99 cm height class. Meanwhile, a few *L. racemosa* individuals in the 1-19 cm size class had grown into larger size classes by 2016.

Mangrove density of the Control Fringe (CF) was higher than in the Treatment Fringe (TF) throughout the surveys, however this was due to a high density of seedlings in CF, whereas larger individuals (sapling and pole size) were more prevalent in the Treatment Fringe plots. Decreased density in the Fringe plots over time showed a thinning of mangrove individuals, and an increase on the dominance of *R. mangle*. Decreased density in the Fringe by 2001 may have allowed for

the increase in seedling establishment by 2016. In the CF plots, *L. racemosa* in the 1-19 cm size class had already thinned out by 2001, and *R. mangle* became the denser species in the 20-59 cm size class with *L. racemosa* and *R. mangle* present throughout the larger size classes. By 2016, the CF density had decreased, while a few individuals attained heights of ~14 m, and seedling size *R. mangle* remained. The TF plots similarly had a decrease in *L. racemosa* density between the census periods, with few *L. racemosa* continuing in the plots beyond the seedling or lower size classes by 2001. By 2016, discounting individuals below 19 cm, the Treatment Fringe had a higher mangrove density in the range of 100-799 cm, which contrasted with the thinning of large mangroves in CF, where a few individuals reached to the 1400-1499 cm size class.

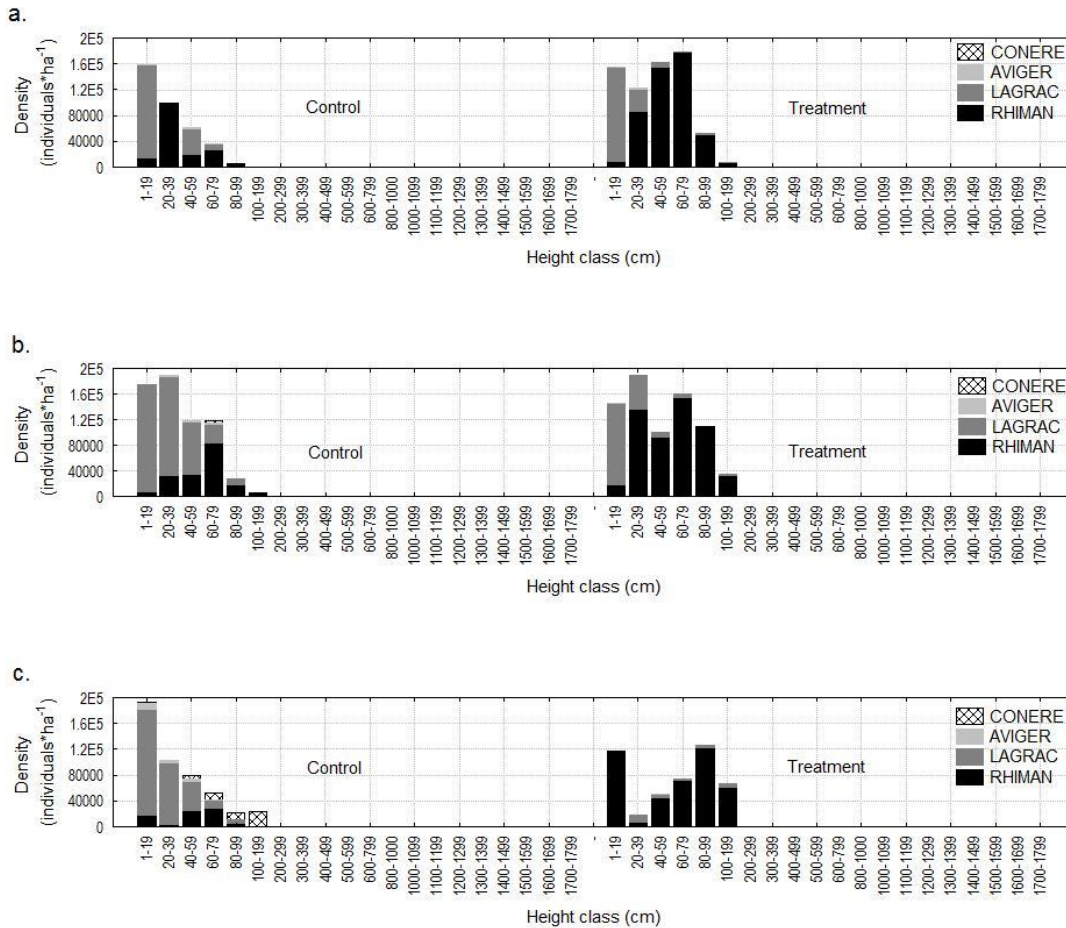


**Figure 1.3.2:** Graph of height distribution of mangrove stems in the Control Dwarf and Treatment Dwarf blocks in (a.) 1996, (b.) 2001, and (c.) 2016 census. Individuals censused in Control and Treatment blocks were summed and an average density by plot area was converted to density per hectare. The 1-19 cm size class is representative of censused mangrove seedlings.

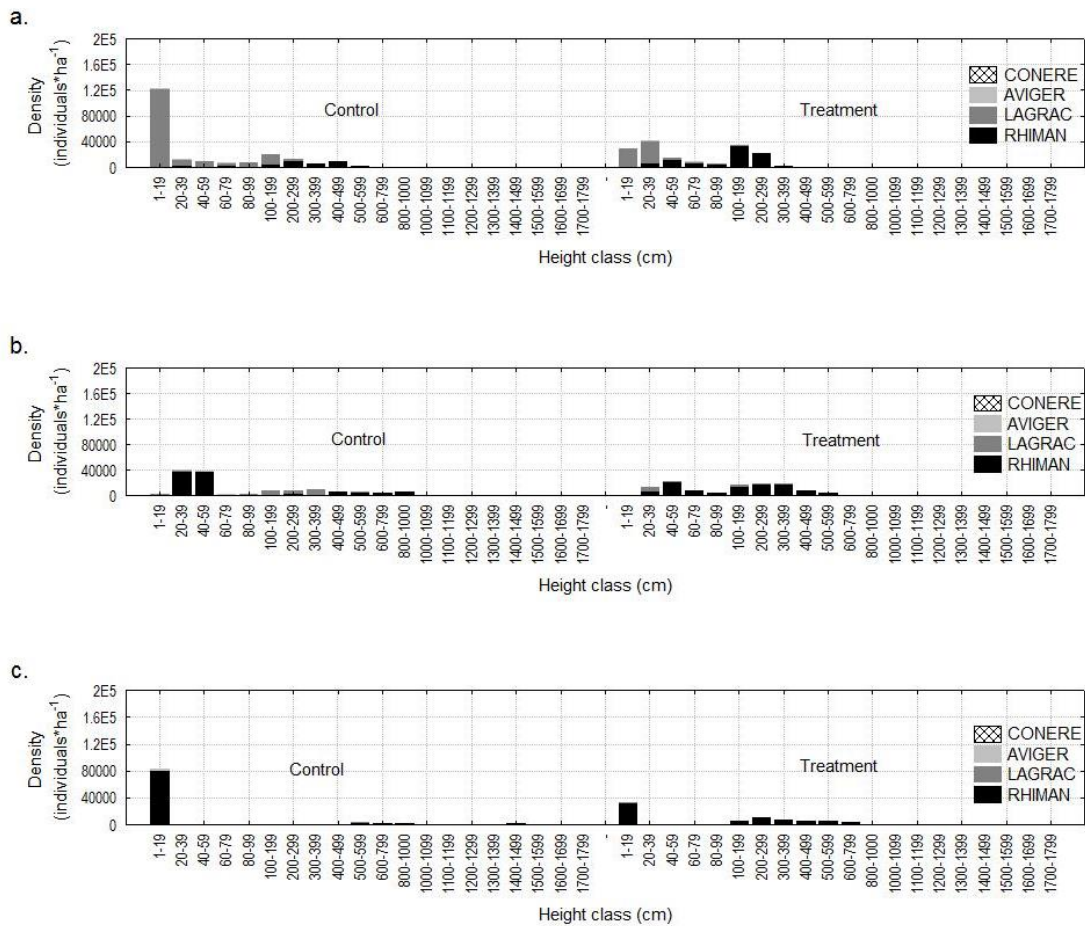


**Figure 1.3.3:** Height distribution of mangrove stems in the L-31E Control Fringe and Treatment Fringe blocks in (a.) 1996, (b.) 2001, and (c.) 2016 census. Individuals censused in Control and Treatment blocks were summed and an average density by plot area was converted to density per hectare. The 1-19 cm size class is representative of censused mangrove seedlings.

On an annual basis from 1990 through 2015, NDVI values derived from 30 m Landsat imagery were extracted for plot locations. Landsat Surface Reflectance-derived spectral indices, calculated from bands of Landsat 4–5 TM and Landsat 7 (ETM+) imagery on single dates, were downloaded from the USGS (<http://earthexplorer.usgs.gov/>). The spectral reflectance data had been processed and atmospherically corrected using the Landsat Ecosystem Disturbance Adaptive Processing System (LEDAPS) (Masek et al. 2006). Only images that were free of clouds and cloud shadows over the L31E study area were chosen between the months of October and early January of each year. As a result, NDVI was available from a cloud-free image in the late wet-early dry season for each year except for 1997. NDVI values were extracted for pixels including and surrounding the location of each sampling plot; 16 pixels in a 4 by 4 arrangement for the fringe plots and 25 pixels in a 5 by 5 arrangement for dwarf mangrove plots. The average value of NDVI for each treatment block for each year was compared to the calculated aboveground biomass in corresponding years of available field data. The sequence of average NDVI values for Treatment Fringe, Control

Fringe, Treatment Dwarf, and Control Dwarf plots were examined to assess the effects of known freeze events and hurricanes.

Throughout most census years, average aboveground biomass ranged from the Control Dwarf at the low end, to the Treatment Dwarf, Treatment Fringe, and Control Fringe with highest biomass (**Figure 1.3.4**). The 2016 census was an exception, with average biomass of TF being greater than the average biomass in CF, although standard error was larger for average CF biomass. Biomass growth in the dwarf plots was very slow in comparison to the fringe, and they even experienced a slight decrease during 2001-2016; however, there was an increase in biomass in all forests since the first 1995 census. In the pre-2001 censuses, biomass of the Control Fringe plots increased more rapidly than in the Treatment Fringe. Although density of TF plots decreased (**Figure 1.3.3**), biomass may have continued to increase due to increased seedling density with the opening of the canopy, and increased contributions of biomass by larger remaining individuals.

In all four forest types (CD, TD, CF, TF), aboveground biomass was predominantly from *R. mangle* in initial censuses. In both Treatment blocks, *R. mangle* continued to comprise most of the forest biomass throughout the census period, with minimal representation from *L. racemosa*. In the CF forests plots, *R. mangle* was also dominant, while the contribution of *A. germinans* to stand biomass was negligible by 2016. CD forest plots continuously had a small amount of *A. germinans* biomass, and by 2016 had nearly equal parts biomass from *R. mangle*, *L. racemosa*, and *C. erectus*, quite contrary to the pattern in the other three forests.

NDVI was highly positively correlated with biomass for the fringe plots ( $R^2 = 0.8$ ; **Figure 1.3.4a**) and had a slightly weaker positive correlation for dwarf plots ( $R^2 = 0.67$ ; **Figure 1.3.4b**). The biomass of all plots, and the associated vegetation index values, have increased over time, despite temporary decreases attributable to disturbance events. In the dwarf mangrove plots, freeze events provide the disturbance that leads to decreases in biomass and NDVI and subsequent recovery. Similarly, after an initial decrease in NDVI following Hurricane Andrew (1992), forest recovery was marked by increasing biomass, which paralleled an increase in the vegetation index.

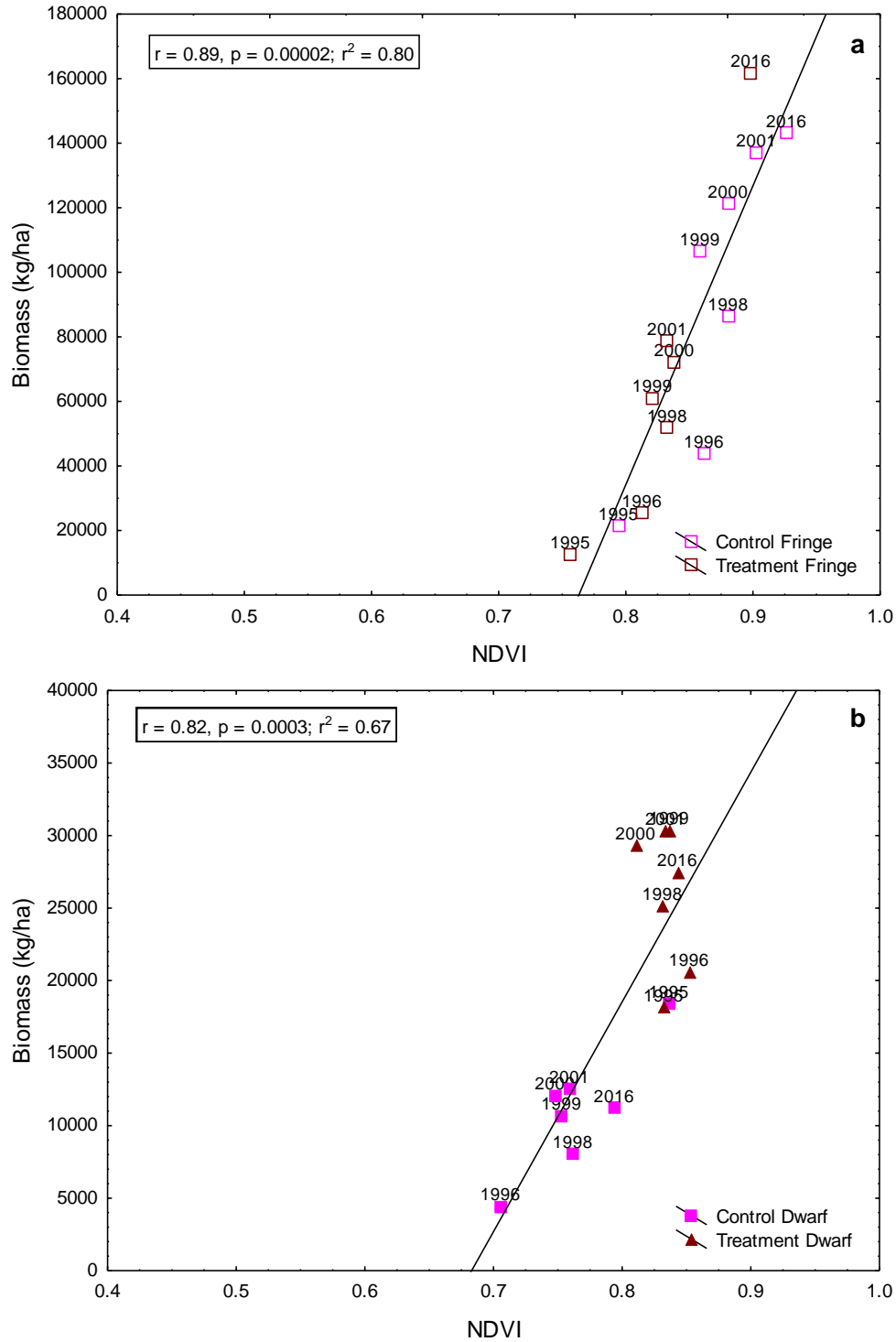


**Figure 1.3.4:** Correlation between NDVI and biomass in a) fringe and b) dwarf sampling plots. Separate for each plot – not the average.

The NDVI of both treatment and control fringe plots decreased by almost 50% of their pre-event index value following Hurricane Andrew (**Figures 1.3.5c and d**). The low biomass estimates of the fringe plots in 1995 at the time of the first field sampling attest to the devastation of this disturbance event. A much smaller decrease in NDVI is observed after the hurricanes of 2005 that

impacted south Florida with winds 30-40 m/s compared to 60 m/s winds from Hurricane Andrew (Powell and Houston 1996). NDVI values recover within one year after the hurricanes of 2005, and while field measurements of biomass were not available immediately before and after, it appears from the response in NDVI that the disturbance's effects on biomass of the plots were minor. Conversely, it took 4 years for NDVI to recover to pre-Andrew values in the fringe mangrove, yet biomass continued to increase for the next decades, especially in the treatment fringe. This increase happened at first quickly, and then slowed down at some time between the field sampling in 2001 and 2016.

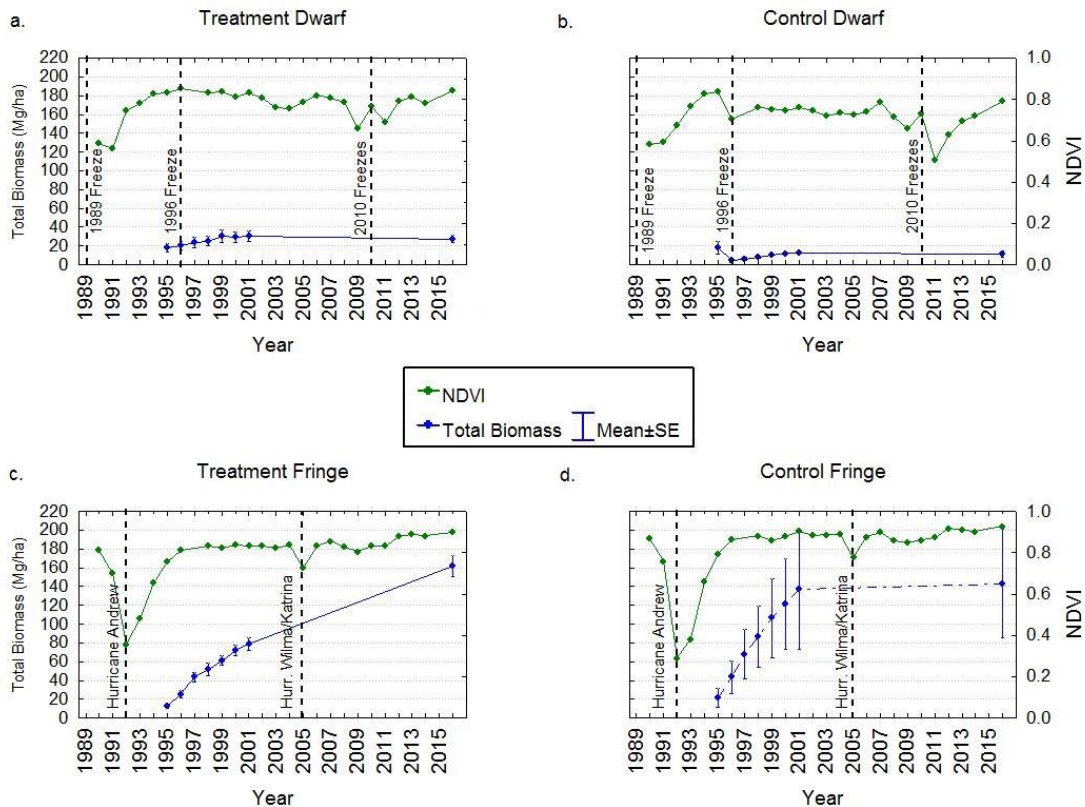


**Figure 1.3.5:** Time series of mean NDVI (1989 to 2016) (right y-axis) compared to mean total biomass (Mg/ha) (1995-2001,2016) (left y-axis) for a) treatment dwarf (n=3), b) control dwarf (n=3), c) treatment fringe (n=4), and d) control fringe (n=4) plots. The timing of Hurricane Andrew (1992) and Hurricanes Wilma and Katrina (2004) are indicated on the fringe plots by dashed lines. Similarly, the timing of freeze events is indicated on the dwarf plots by dashed lines.

In the dwarf mangroves, effects of hurricanes were not evident and this is likely a function of low canopy height of these forests (Zhang et al. 2016). Instead, severe freezes provide a recurring disturbance event in forests of this stature. Both the freezes from 1989 and 2010 are recorded in the NDVI of both the control and treatment dwarf plots (**Figures 1.3.5a and b**). However, effects of freeze event can be localized, causing damage in some locations but not others. This phenomenon is depicted in the decrease of biomass and NDVI to the 1996 freeze event in Control Dwarf plots, while nearby Treatment Dwarf plots were not impacted by the freeze.

## 2. Environmental and paleo-indicators

### 2.1. Diatom patterns in surface sediments

#### *Introduction*

The main objectives of the 2016-2018 survey of diatom communities at 55 locations in coastal wetlands of the southeastern and southern Everglades are to: 1) determine environmental drivers of assemblage composition in order to 2) develop diatom-based inference models that could be used to track trajectories of environmental change over time. We expect that changes driven by saltwater intrusions into coastal zone caused by sea level rise and anthropogenic alterations of hydrodynamic conditions in this region will be evident based on diatom assemblages preserved in ~1-meter-long sediment cores collected along pre-defined transects.

In March and April, 2016, we surveyed diatom communities at 21 locations along 8 transects positioned perpendicularly to Florida Bay and Biscayne Bay (Fig. 2.1.1). 4 sites located east of the L31E Canal between Mowry and Military Canals, concentrated in an area of remnant coastal wetlands now dominated by dwarf red mangroves, had been previously surveyed in 2000-2002 (Gaiser et al. 2005). The other sites surveyed in 2016 overlapped with the transects created for the 1993-94 study of vegetation and soils at 56 sites in the Southeast Saline Everglades (SESE) (Meeder et al. 1996).





**Figure 2.1.1:** Sampling locations of diatoms along transects in coastal wetlands of the SE Everglades.

## ***Methods***

### *Laboratory Methods*

Carbonate and organic materials were eliminated from diatom subsamples by adding ~20 ml of a concentrated (70%) nitric acid to the subsamples. The subsamples were left in the acid under the fume hood overnight and then heated up to speed up the dissolution process. Next, the acidity of the samples was lowered to pH 7 (neutral) by decanting them with DI water at least 6-8 times every 12 hours. The cleaned diatom samples were stored in 10 ml glass vials and preserved with a few droplets of alcohol. For each sample, approximately 1 ml of slurry was placed on No.1 coverslips, air dried and mounted onto glass slides using Naphrax®. At least 300 diatom valves were counted on random transects across each slide using a Nikon E400 light microscope at 788x magnification (N.A. = 1.4). Valves were identified according to the local and standard diatom taxonomic literature.

### *Statistical methods*

Abundance of each taxon was expressed as a proportion of the total valve counts in each sample. All data were arcsine square root transformed to down-weight the importance of very abundant species and to ensure that rarer species also contributed to the results. Compositional similarity among sites was determined using hierarchical clustering with the Sørensen distance measure and flexible beta ( $\beta = -0.25$ ) linkage method, and visualized in one-way and two-way dendrograms, and nonmetric multidimensional scaling ordination diagrams. The statistical significance of differences in diatom assemblage structure among groups defined by cluster analysis were tested using the Analysis of Similarities (ANOSIM) procedure. Relationships between distance from the coast and assemblage structure were represented by a vector in the NMDS.

## Project Findings

A total of 95 diatom taxa were recorded at 21 sites. Species richness significantly decreased with distance from the coast (**Figure 2.1.2**). Species density ranged from 8 taxa per slide at the most distant site (M5N, 11.6 km from the Florida Bay coast in the SW part of the oligohaline Everglades) to 30 taxa at the site closest to the coast (TDE, east of the L31E Canal and 280 m from the Biscayne Bay coast). After removing rare taxa, 48 taxa remained in the database that were used in further analyses.

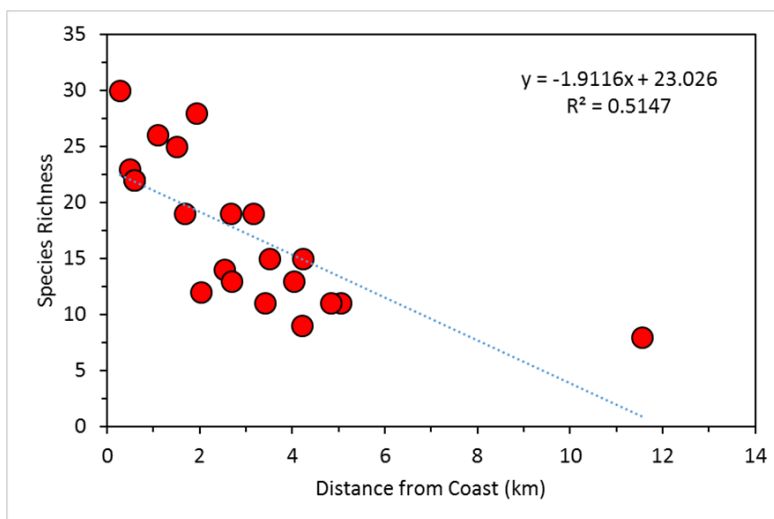


**Figure 2.1.2:** Significant negative correlation between species richness and distance from coast.

Cluster analysis revealed significant differences in diatom assemblages among sites and regions. Two major clusters and 6 subclusters with distinct diatom assemblages were identified by the analysis (**Figure 2.1.3, 4 and 6**). Sites in Cluster 1 were characterized by abundant oligohaline to mesohaline taxa, which were mostly absent from the sites in Cluster 2 (**Figure 2.1.3-6; Table 2.1.1; Plate 2.1.1**). Cluster 2 was characterized by high abundance of meso- to polyhaline taxa (**Figure 2.1.3-6; Table 2.1.1; Plate 2.1.1**). Taxa indicative of freshwater Everglades marshes (e.g., *Encyonema evergladianum*, *Mastogloia calcarea* or *Brachysira neoexilis*), were absent from sites in Cluster 2 (**Figure 2.1.5; Table 2.1.1; Plate 2.1.1**). Cluster 1 comprised distant from the coast sites, located north of the “white zone” or in the transitional zone between the “white zone” and freshwater wetlands, while Cluster 2 contained sites located in closer proximity to the coast, mostly in the “white zone” (**Figure 2.1.1**). Sites in Clusters 1 and 2 were characterized by distinct diatom assemblages, which corresponded to distinct physico-chemical and hydrologic conditions at the sites, and distinct vegetation patterns (**Figure 2.1.3, 4 and 6**).

An ANOSIM test revealed that the differences in diatom composition were significant between Clusters 1 and 2 ( $R = 0.767$ ;  $p = 0.001$ ), which was also captured in the 2-dimensional NMDS (**Figure 2.1.4 and 5**). Assemblages in Subclusters 1a and 1b different significantly from each other ( $R=0.759$ ;  $p=0.012$ ) (**Figure 2.1.3 and 4**). Differences in the structure of assemblages among subclusters in Cluster 2 were only significant between Subclusters 2a and 2d, and 2b and 2d (**Figure 2.1.3 and 4**).

Indicator Species Analysis (ISA) identified 17 taxa as indicative of the 6 Subclusters (**Table 2.1.1**). Indicator taxa in Subclusters 1 and 2 were associated with areas distant from the coast, characterized by oligo- to mesohaline conditions, while indicators of the remaining groups of sites were associated with areas in close proximity to the coast, characterized by mostly polyhaline conditions (**Table 2.1.1; Figure 2.1.7**). The highest number of indicator taxa was associated with Subclusters 1 and 4, the former representing the furthest from the coast sites (~3.5-11.5 km) while the later positioned < 2 km away from the coast (**Table 2.1.1; Figure 2.1.7**).

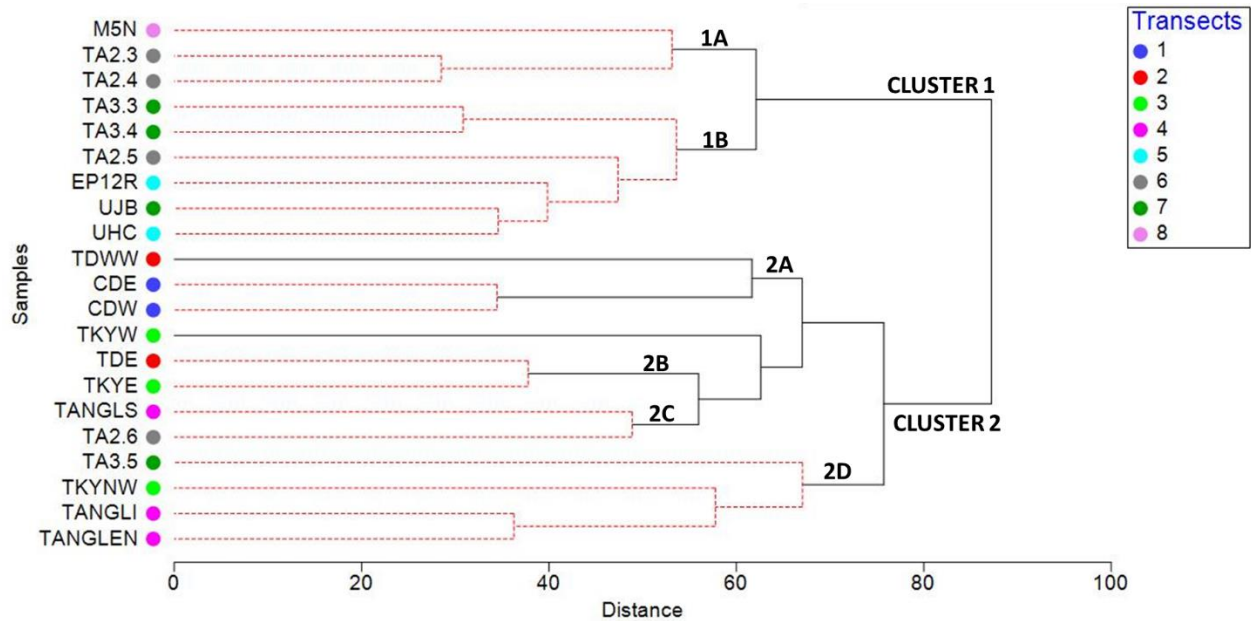


**Figure 2.1.3:** Spatial differences in diatom communities determined using cluster analysis.

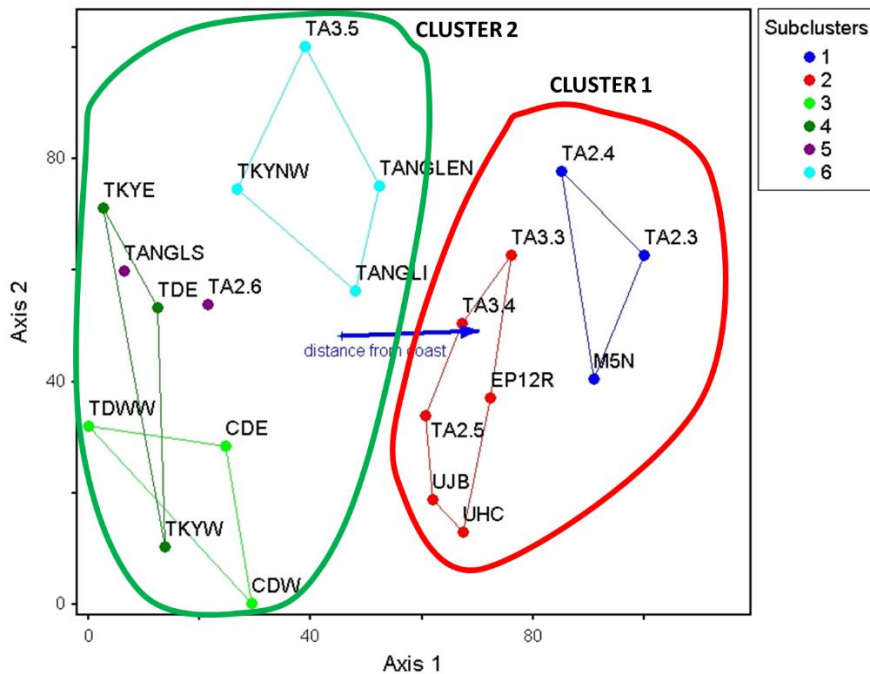


**Figure 2.1.4:** Non-metric multidimensional scaling ordination diagram showing distinct diatom communities identified using cluster analysis. The point cluster was rotated around the centroid to maximize the correlation of a distance variable with the horizontal axis 1.

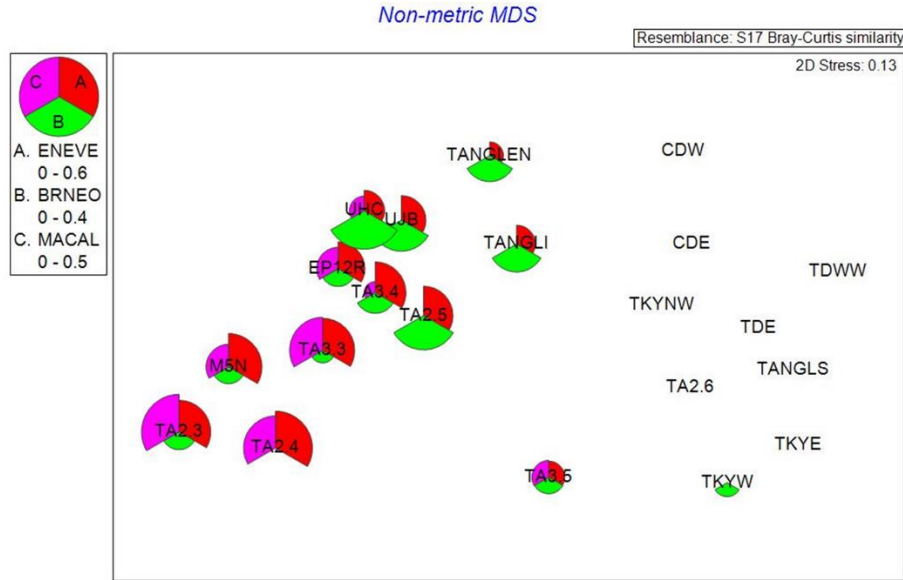


**Figure 2.1.5:** Non-metric multidimensional scaling ordination diagram showing distinct diatom communities and the relative abundance of oligohaline indicator taxa *Encyonema evergladianum* (ENEVE), *Brachysira neoexilis* (BRNEO), and *Mastogloia calcarea* (MACAL).

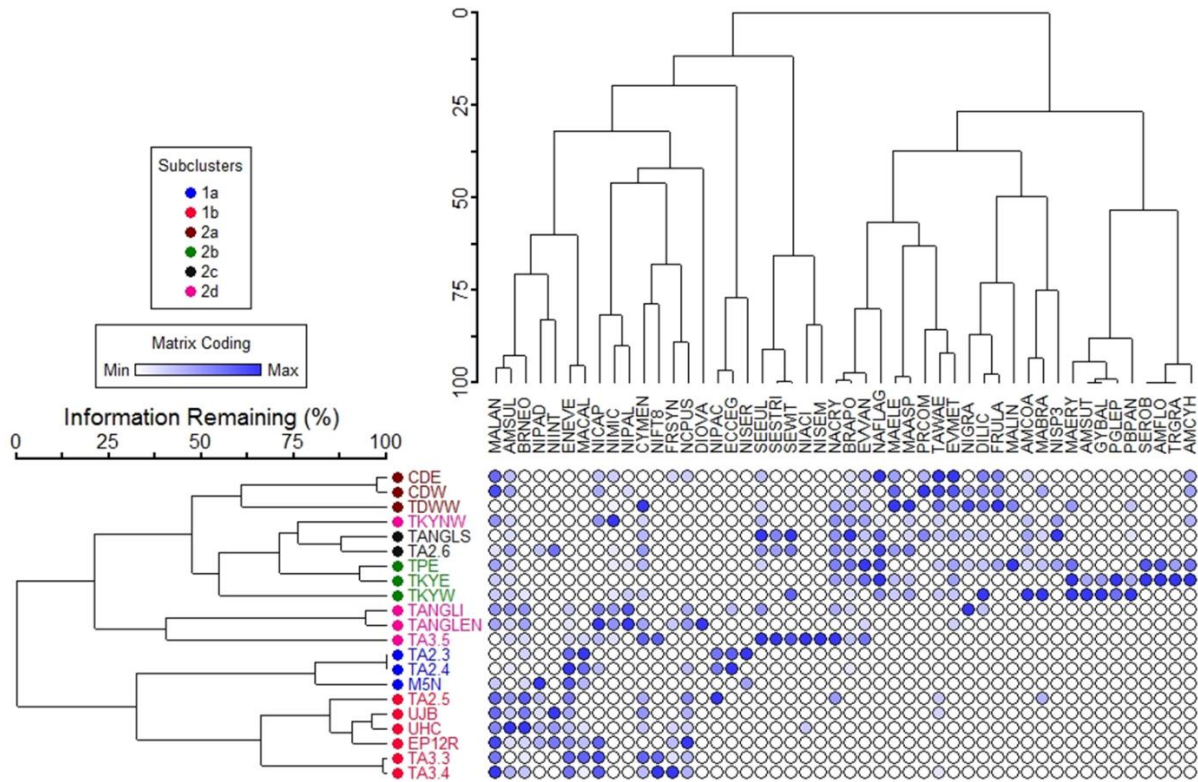


**Figure 2.1.6:** Two-way cluster dendrogram showing the abundance of the taxa used in analysis among sites and subclusters defined by cluster analysis. (abbreviations for indicator taxa defined in **Table 2.1.1**).

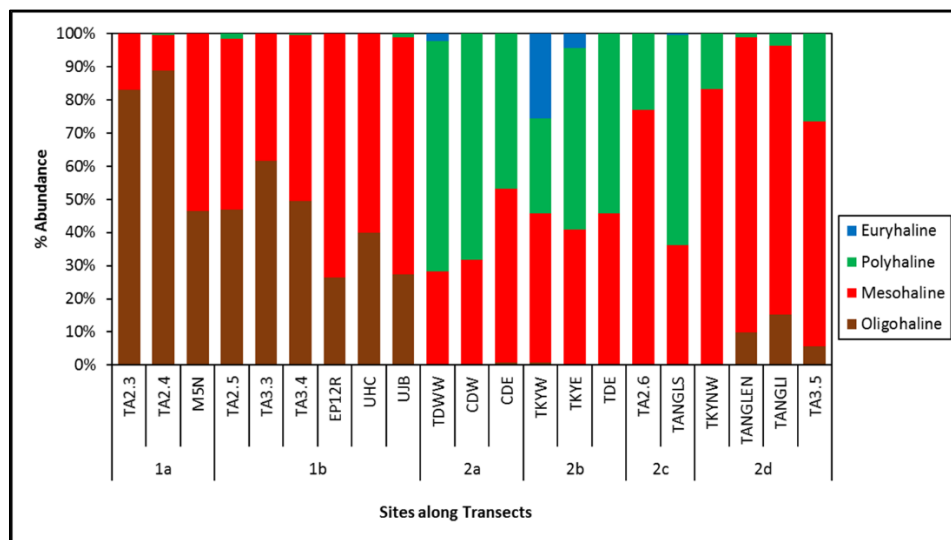


**Figure 2.1.7:** Percent abundance of taxa with different salinity tolerances at the study locations. Sites are grouped by subclusters and clusters. Taxa tolerances are based on optima and tolerances defined in the previous studies of diatom communities in the South Florida region. Salinity categories: Oligohaline (0.5- <5 ppt); Mesohaline (5- <18 ppt); Polyhaline (18- <30 ppt); Euryhaline (30- <40 ppt).

**Table 2.1.1:** Indicator taxa for different subclusters defined by cluster analysis. Salinity categories: O = oligohaline (0.5- <5 ppt); M = Mesohaline (5-18 ppt); P = Polyhaline (18- <30 ppt).

Indicator Taxa	Salinity Category	Subcluster	Observed Indicator Value	p-value
<i>Mastogloia calcarea</i>	O	1a	71.8	0.002
<i>Nitzschia semirobusta</i>	M	1a	66.7	0.044
<i>Encyonopsis cf. cesatii var. geitlerii</i>	O	1a	58.8	0.044
<i>Encyonema evergladianum</i>	O	1a	54.7	0.000
<i>Navicella pusilla</i>	M	1b	53.6	0.005
<i>Brachysira neoexilis</i>	O	1b	51.9	0.014
<i>Tabularia waernii</i>	P	2a	64.4	0.002
<i>Mastogloia elegans</i>	P	2a	62.4	0.023
<i>Envekadea metzeltinii</i>	P	2a	53	0.029
<i>Mastogloia erythraea</i>	P	2b	84.2	0.004
<i>Seminavis robusta</i>	P	2b	66.7	0.045
<i>Amphora floridiana</i>	P	2b	66.7	0.045
<i>Tryblionella granulata</i>	P	2b	66.7	0.045
<i>Seminavis strigosa</i>	P	2c	68.6	0.017
<i>Seminavis witkowskii</i>	P	2c	63.5	0.030
<i>Seminavis eulensteinii</i>	P	2c	51.4	0.048
<i>Nitzschia microcephala</i>	M	2d	69.3	0.010

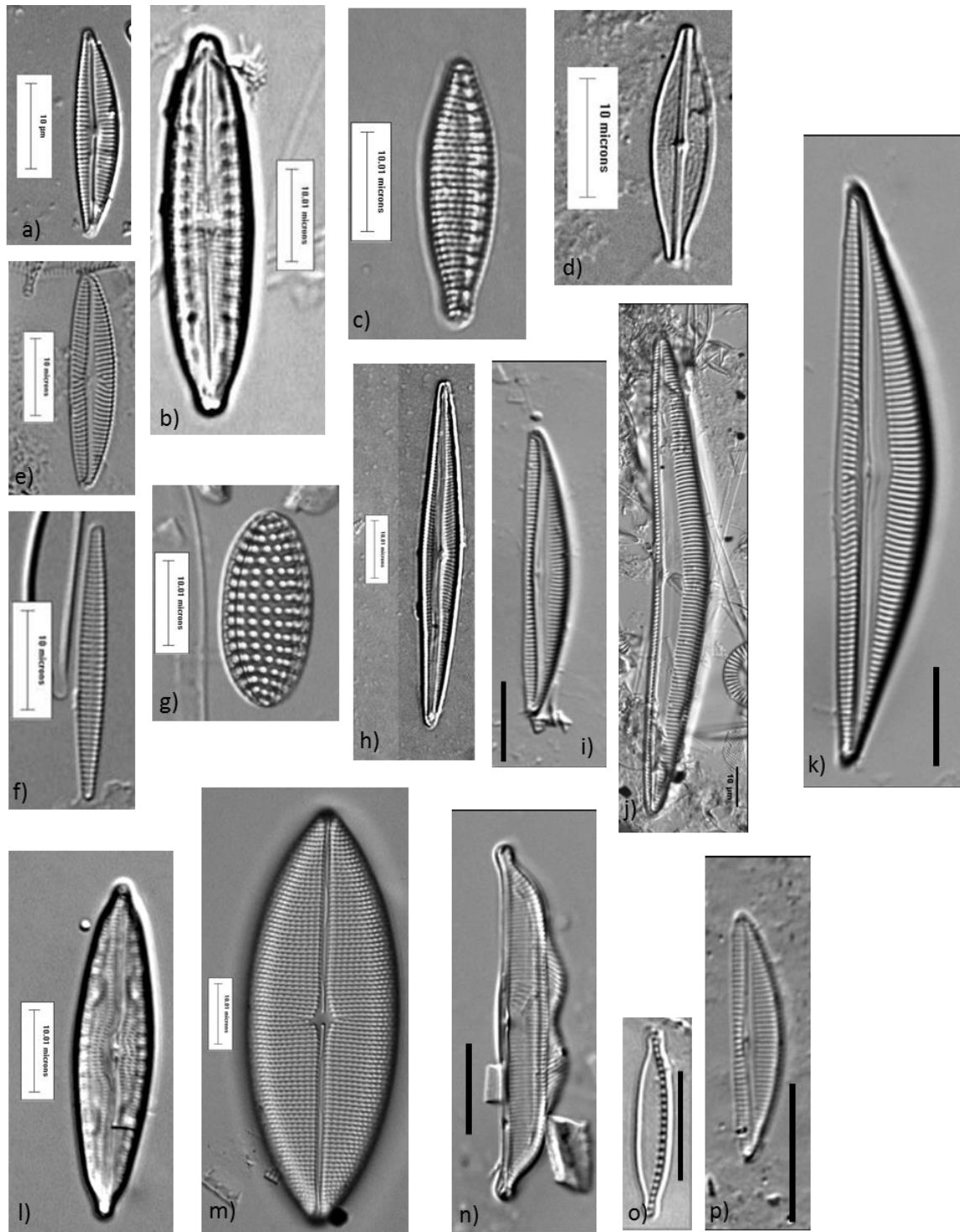


**Plate 2.1.1:** a) *Encyonema evergladianum*; b) *Mastogloia calcarea*; c) *Nitzschia semirobusta*; d) *Brachysira neoexilis*; e) *Navicella pusilla*; f) *Tabularia waernii*; g) *Triblionella granulate*; h) *Encyonopsis cf. cesatii* var. *geitlerii*; i) *Seminavis witkowskii*; j) *Seminavis eulensteinii*; k) *Seminavis robusta*; l) *Mastogloia erythraea*; m) *Mastogloia eleans*; n) *Amphora floridiana*; o) *Nitzschia microcephala*; p) *Seminavis striatose*; r) *Envekadea*

## *Discussion and Conclusions*

Earlier studies showed that the fresh-brackish water ecotone lining the south and southeast coast of Florida is migrating rapidly inland affecting water chemistry and vegetation patterns (Ross et al. 2000, 2001). These changes are also slowly restructuring microbenthic algal communities in this region. Previous studies showed that salinity has an overriding control on diatom community composition throughout south Florida coastal wetlands and estuaries (Gaiser et al. 2005; Wachnicka et al. 2010, 2011). Unlike measurements of individual water quality variables, diatoms not only capture the effect of salinity on biota, but they also capture the interactive effect of multiple stressors on biota. These valuable characteristics make them more reliable indicators of ecosystem status than episodic water quality measurements, since the latter do not always capture fluctuations in physicochemical water conditions caused by numerous drivers of change. Therefore, the sensitivity of diatoms makes them ideal to study the effect of saltwater encroachment on coastal ecosystems in this region, and to determine the rate of these changes.

With the 2016 study of modern diatom assemblages at 21 coastal locations, we took the first step to better understand their association with different vegetation communities and hydrologic conditions in the coastal zone. Our survey revealed that they are organized into distinct oligomesohaline and poly-euryhaline assemblages. The structure of the assemblages changed with distance from the coast, which also implies changes in physico-chemical conditions and vegetation patterns.

Considering the scarcity of continuous salinity recording in the vast areas of the coastal Everglades, diatoms provide an ideal tool not only for salinity monitoring as saltwater intrusions continue to spread farther inland, but also for restructuring past environmental conditions from fossil diatom assemblages preserved in the sediment cores collected during the 2016 survey, as well as those that will be collected during 2017/2018 surveys. An initial examination of a few samples from one of the cores collected from a coastal location revealed the presence of well-preserved diatom assemblages in the core samples. Therefore, a very rare opportunity exists to use diatoms, which have already proven to be a powerful tool in salinity reconstructions in the nearshore areas of Biscayne Bay, Florida Bay and Shark River Slough (Wachnicka et al. 2013a,b,c; 2015), to study the effects of saltwater encroachment and ecosystem dynamics in the coastal zone of the southern Everglades.

During 2017/2018, we will continue surveying modern diatom communities at the remaining 25 locations to further improve our knowledge of diatom assemblages, and their association with different plant communities and environmental conditions across the coastal zone. These data may also allow us to develop inference models to reconstruct past environmental conditions based on diatom assemblages preserved in sediment cores in the future.

### **2.2. Mollusk composition in sediment profiles**

#### *Introduction*

We report on three cores which represent a temporal and spatial transect of coastal influence adjacent to the Mowry Canal (C103) (**Figure 2.2.1**). The area has been receiving fresh water

discharge from the L-31E since 1996. Between 1996 and 2014, discharge was minimal, but since 2014 the volume of water delivered into the mangrove basin has increased substantially.



**Figure 2.2.1:** The Mowry Canal transect.

## ***Methods***

Cores were collected and processed for sediment constituents to determine the present and changes in depositional environment and mollusks for development of the salinity index.

Sediment analysis was performed on 1 cm intervals from all cores. The core increments were weighed immediately after sub-sampling while frozen to determine wet bulk density. After thawing, the sample was split into two halves, and one half was used for sediment analysis. A one cubic centimeter sample was separated and used to calculate dry bulk density, organic content (OC) and carbonate content (Meeder et al. 1996). The remainder of the sample was washed thru sieves and types of organic material were sorted, dried and weighed. Sediment analysis was done at two levels: (1) gross sediment characteristics, including bulk density, total carbonate and total OC, and (2) detailed accounting of the organic fraction, achieved by separating and weighing by plant species, organ type (cable root, rootlets, stems, leaves, bark and flowers), and amorphous material (i.e., fine grained unidentifiable organic material).

One half of each sample was washed through sieves and all invertebrates over 1mm in size were collected. All specimens were identified and counted in order to calculate a Salinity Index (Meeder et al. 1996). The sediment data for the three cores are described below.

## ***Project Findings***

**Core TDWW.** This core was collected ~ 25 m east of the levee (**Figure 2.2.1**) and extended to bedrock. The core exhibits no compaction and includes the accumulated floc on the scrub mangrove basin surface (**Figure 2.2.2**). This is the longest core collected. The core is predominantly comprised of carbonate mud and organic material. Average CaCO<sub>3</sub> content of 1

cm sub-samples in TDWW was 83.2 % of the sample weight, while OC content was 16.8 % (Figure 2.2.3). The density differences between OC and CaCO<sub>3</sub> is considerable. OC material is considerably less dense than water and CaCO<sub>3</sub> (marl) may be twice as dense than water. OC is most abundant in the upper part of the core, where mangrove constituents were observed. OC varied between 6 and 78% of total sub-sample weight. The marl sediments in the middle of the core was low in OC content (6 to 12 %); in contrast, in the lower portion of the core, in which sawgrass material was observed, OC content ranged from 12 to 21 %.

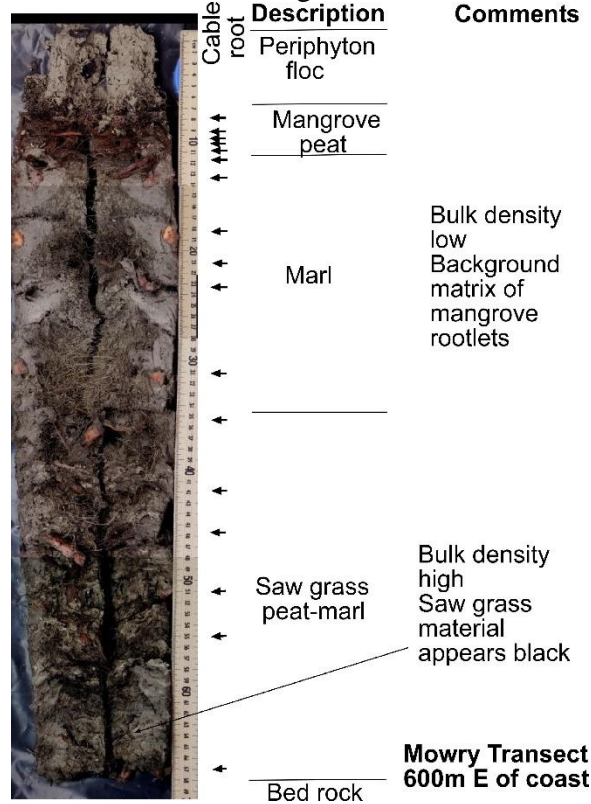


**Figure 2.2.2:** TDWW core shows thin peat with abundant cable roots at top overlying a peat-marl with low cable root density. This core demonstrates that mangrove presence occurred long before peat development.

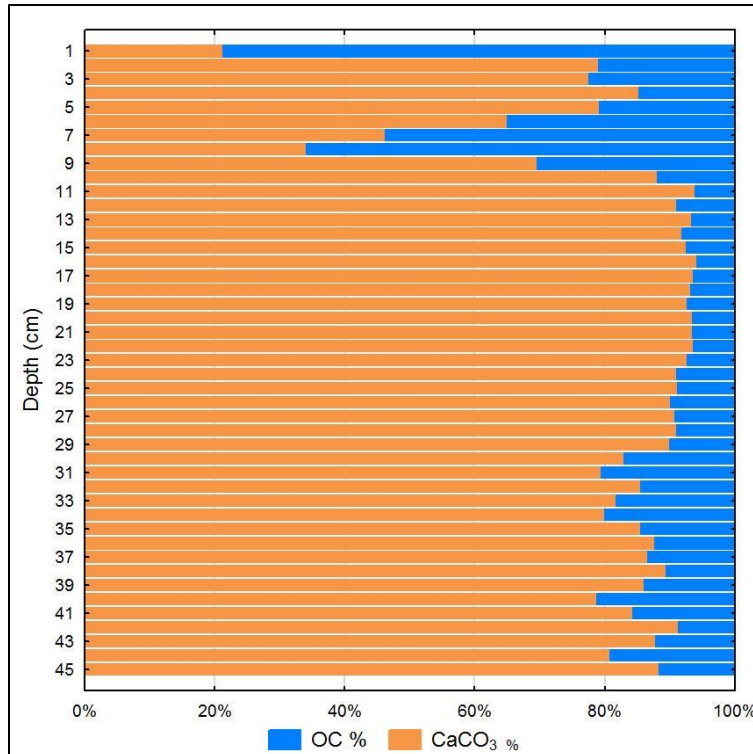


Figure 2.2.3: Average CaCO<sub>3</sub> and OC content of 1 cm sub-samples in TDWW core.

The water content (total weight - dry weight) showed little change in intervals 2-10 and 22-45 cm in TDWW, but was higher and more variable between 11 and 21 cm depth (Figure 2.2.4). This suggests only minor compaction as compaction requires loss of water. The variability found in the core interval between 10 and 22 cm may be the result of the presence of dead cable roots, which contain considerable water.

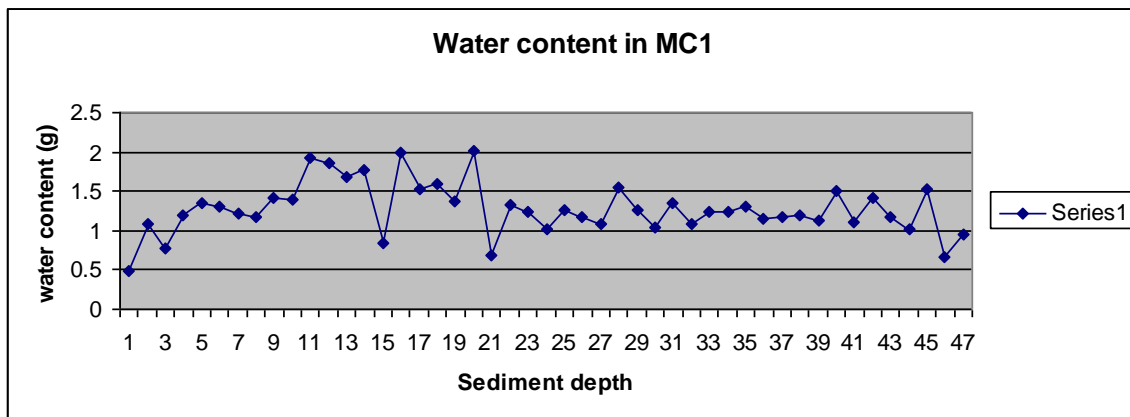
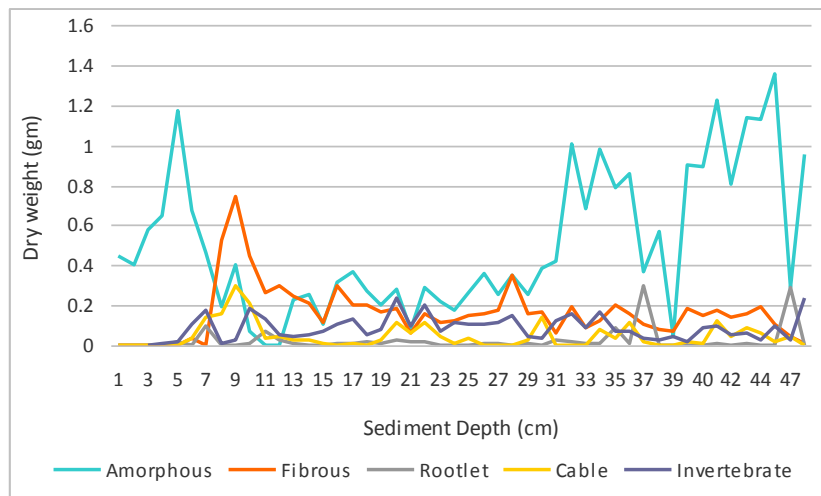


Figure 2.2.4. Water content in TDWW. Very little change between 22 and 45 cm.

The major organic constituents (cable roots, rootlets, fibrous, amorphous) varied with depth (Figure 2.2.5), as did the plant species of origin. Significantly, sawgrass remains were found only at the surface and in the bottom 30 cm of the core. Mangrove cable roots were found along numerous strata (arrows) throughout the core, documenting the presence of mangroves for the entire time span of the sediment deposition. Observations during the excavation of several

mangrove clumps in marl substrate revealed only horizontal cable roots without any downward trending roots in contrast to occasional downward trending roots in peat substrates. Mangrove peat is beginning to develop in the upper few cm. This documents a substantial lag between mangrove colonization and peat development. Invertebrate skeletal material varied little throughout the core. Exceptions were increases in mass with storm deposition and loss of skeletal material by dissolution in intervals with mangrove peat.

Fibrous and rootlet material varied little between 11 and 48 cm. An increase beginning at ~ 11 cm was the result of increasing mangrove presence (**Figure 2.2.2**). (Note: samples were lost in processing in the upper 7 cm, which was approaching peat). The amorphous content was highest between 30 and 48 and 0 and 8 cm which appears to be related to the distribution of sawgrass material in the core, though this relationship is not yet understood.



**Figure 2.2.5:** Distribution of organic constituents in TDWW.

**Core TDE.** The upper 16 cm of the TDE core (**Figure 2.2.6**) was mangrove peat, However, mangrove cable roots were found considerably deeper in the core than peat, suggesting that mangroves were present for considerable time prior to peat development. Cable root density appears to control peat development, as cable root density increased with increasing OC. This is illustrated when comparing TDWW (**Figure 2.2.2**) to TDE (**Figure 2.2.6**).



**Figure 2.2.6:** Upper portion of Core TDE, exhibiting gradual transition from marl to mangrove peat. Grey carbonate mud decreases upwards to nearly pure peat at ~16 cm.

The water content of TDE varied little but decrease slightly upwards (**Figure 2.2.7**). Minor variations are most likely attributed to the presence of dead cable roots that contain considerable water. The decreasing trend toward the top of the core is unexplained at this time.

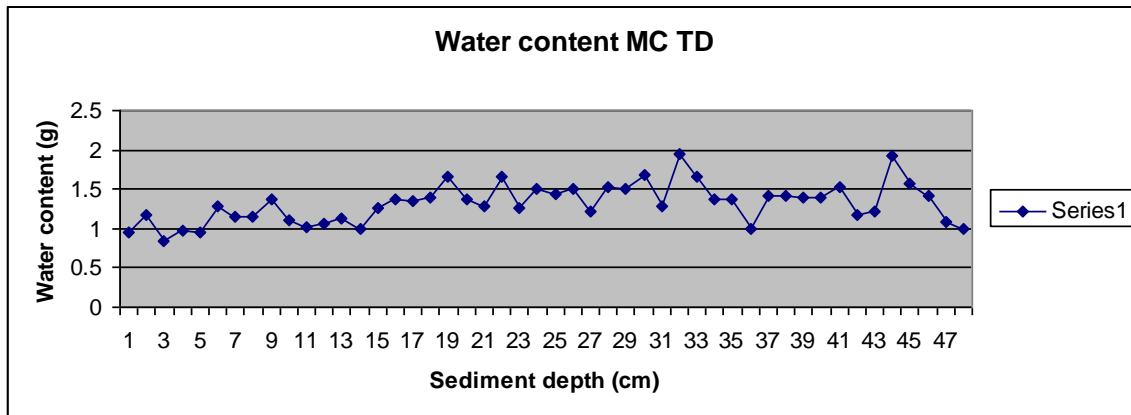


**Figure 2.2.7:** Water content in sub-samples of TDE.

**Core TF.** Core TF is comprised of very pure mangrove peat. The core never penetrates beyond the peat (**Figure 2.2.8**).



**Figure 2.2.8:** Core TF, 20 m inland from Biscayne Bay, located on a natural coastal levee.

**Salinity analysis.** All mollusks were identified in 1cm increments. Species were counted and assigned a salinity tolerance from 1 to 5 based on descriptions of their ecological niche in the literature (**Table 2.2.1**). From this data a salinity index (SI) was calculated for all 1cm sediment intervals in each core, based on weighted averages of species densities in each 1 cm sample (**Table 2.2.2**).

**Table 2.2.1:** Mollusk species and their salinity ranking. (from Meeder et al. 1996).  
Ranks: 1, freshwater species; 1.5, freshwater species with tolerance for low salinity; 2, brackish species; 2.5, brackish species that tolerate marine conditions; 3, restricted marine with tolerance for lower salinity; 4, marine species with a tolerance for low salinity; 5, marine species.

Species No.	Species	Salinity Rank	Species No.	Species	Salinity Rank
1	<i>Biomphalaria havanensis</i>	1	17	<i>Turbonilla spp.</i>	4.5
2	<i>Cylindrella spp.</i>	1	18	<i>Alvania spp.</i>	5
3	<i>Laevapex pennisulae</i>	1	19	<i>Anomalocardia auberiana</i>	5
4	<i>Physella cubensis</i>	1	20	<i>Bulla striata</i>	5
5	<i>Planorbella scalaris</i>	1	21	<i>Caecum pulchellum</i>	5
6	<i>Polygyra spp.</i>	1	22	<i>Carditas spp.</i>	5
7	<i>Pomacea paludosa</i>	1	23	<i>Chione cancellata</i>	5
8	<i>Littoridinops monoroensis</i>	1.5	24	<i>Chione latilirata</i>	5
9	<i>Pyrogophorus platyrachis</i>	2.5	25	<i>Corbula contracta</i>	5
10	<i>Cerithidea beattyi</i>	3	26	<i>Lima pellucida</i>	5
11	<i>Batillaria minima</i>	4	27	<i>Marginella spp.</i>	5
12	<i>Brachidontes exustus</i>	4	28	<i>Meioceras nitidum</i>	5
13	<i>Cyrenoida floridana</i>	4	29	<i>Retusa sulcata</i>	5
14	<i>Littorina angulifera</i>	4	30	<i>Rissoina catesbyana</i>	5
15	<i>Melampus coffeus</i>	4	31	<i>Strigilla carnaria</i>	5
16	<i>Terebra dislocate</i>	4.5	32	<i>Tricolia bella</i>	5

**Table 2.2.2:** Salinity index values for Mowry Transect Cores. nm = no identifiable mollusks present, nd = no data and inc = incomplete sample.

Depth (cm)	Site		
	TF	TDE	TDWW
1	nm	nm	1.8
2	nm	nm	1.52
3	nm	nm	1.6
4	nm	nm	1.69
5	nm	nm	1.62
6	nm	nm	1.62
7	nm	nm	1.99
8	nm	nm	2.3
9	nm	nm	1.86
10	nm	nm	1.76
11	nm	nm	Nd
12	nm	nm	1.68
13	nm	nm	1.59
14	nm	nm	1.37
15	nm	2.03	1.29
16	nm	2.18	1.37
17	inc	1.83	1.43
18	4	2.1	1.22
19	3.37	2.68	1.38
20	2.67	1.62	1.41
21	2.37	1.58	1.35
22	3.44	2.09	1.41
23	1.87	1.58	1.41
24	1.5	1.39	1.42
25	2	1.39	1.39
26	nd	1.51	1.42
27	nd	1.57	1.4
28	nd	1.54	1.36
29	nd	1.32	1.36
30	nd	1.4	1.46
31		1.33	

## TDWW salinity profile

The SI profile for core TDWW indicates that sediments from the base of the core to approximately sediment interval 13 cm beneath the surface were deposited in fresh water, i.e.,  $SI \leq 1.5$  (**Figure 2.2.9**). Core 1 was collected 25 m east of L31E in the scrub mangrove basin, and was dominated by marl sediments which are changing to peat-marl. Based on a sediment accumulation rate of  $1.2 \text{ mm yr}^{-1}$  (Meeder et al 1996, **Figure 2.2.3**), or  $8.3 \text{ yr cm}^{-1}$ , this subsoil interval represents  $\sim 133\text{yr}$ . The salinity index increased to a peak in sediment interval 7-8 cm, then dropped to levels barely classified as deposited in a saline environment.

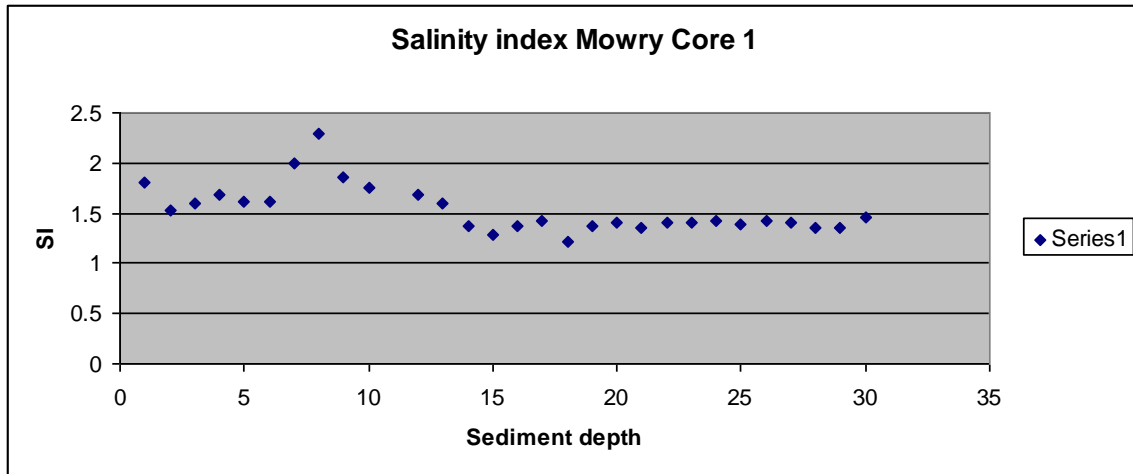


**Figure 2.2.9:** Salinity Index profile for TDWW.

Several fresh water mollusks, such as *Planorbella scalaris*, do not tolerate elevated salinity and are highly useful in determining paleosalinity (**Figure 2.2.10**). In contrast, the dominant gastropod species is the hydrobiid, *Littoridinops monoroensis*, which may occur in either fresh or brackish water, and therefore is assigned an SI of 1.5. Any SI values greater than 1.5 in **Figure 2.2.9** are considered to be influenced by marine water.



**Figure 2.2.10:** An "in situ" specimen of the fresh water gastropod, *Planorbella scalaris*, found in marl at 45 cm in core TDWW. Note another specimen, oriented sideways just above the exposed gastropod.

**TDE salinity profile.** The SI profile is not plotted but is presented in **Table 2.2.2**. The upper 23 cm of the profile is dominated by a marine-influenced molluscan assemblage, and mollusks are missing in the upper 14 cm by dissolution. Marine influenced conditions began with the first appearance of abundant mangrove cable roots (see **Figure 2.2.6**, ~19 cm depth).

**TF salinity profile.** This SI profile is not plotted but is found in **Table 2.2.2**. The SI remains well within the marine influenced range throughout the core. The sediment throughout is mangrove peat.

### *Discussion*

**Core sampling methods.** Pull apart split cores provide much more detail than cut cores. Fine textures that are invisible when cut show up well when the core is split by pulling apart the core (**Figure 2.2.11**).



**Figure 2.2.11:** Fresh water marl interval underlying thin layer of mangrove peat in Core TDWW (Figure displaying a very fine texture of marl with a visible network of mangrove rootlets).

**Sediment compaction.** Compaction can occur during sampling but is also a natural process which is associated with dewatering, decomposition and/or compression of soft tissue. The difference between wet and dry bulk densities is water content (**Figure 2.2.4**). Water content is significant in our analysis because it is useful in determining compaction, especially in peat sections. Where water content doesn't change much down section there can be little compaction, as compaction requires water displacement. There is little evidence for natural compaction based upon water content (**Figure 2.2.4 and 7**). Cores do exhibit voids from cable root decomposition which maintain their shape, again suggesting the absence of compaction (**Figure 2.2.12**). Sometimes these voids, when found within the active root zone, are filled with a later generation of roots that take advantage of the space and route for expansion.

Core 2:400m

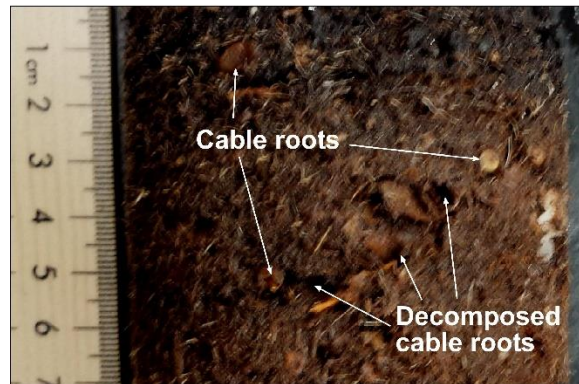


**Figure 2.2.12:** Cable roots in mangrove peat, as well as voids where cable roots have decomposed. Note that the voids are the same shape as the cable roots and show no signs of compaction. This core interval was from 20 to 27 cm below the surface in Core TDE. Such voids are often found at the bottom of deeper mangrove cores not included in this study.

**Differences in sediment types.** Marl is considerably denser than mangrove peat. Marl is  $\sim 2.0$   $\text{mg}/\text{cm}^3$ , while peat is lighter at  $< 1.0$   $\text{gm}/\text{cm}^3$ . A problem in visual interpretation stems from mixtures of marl and peat, as a little marl makes the peat sample much denser. When peat and marl weigh about the same, and density equals  $\sim 1.5$   $\text{mg}/\text{cm}^3$ , the sample looks more like peat than marl. If there is more peat than marl the sediment is termed marl-peat, if marl is more abundant than it is termed peat-marl. The ultimate source of marl is dissolved limestone; the periphyton mat induces precipitation of the dissolved calcium, forming very fine calcite grains which accumulate to form marl.

Mangrove peat is formed in our study area by nearly 100% below ground biomass accumulation. Although the abundance of cable roots (**Figures 2.2.2, 6 and 11**) determines peat development, the groundmass of rootlets makes up the bulk of peat. Root biomass, i.e., cable roots plus rootlets, is considerably higher in peat than marl soils, with the largest difference being in the biomass of cable roots (**Figures 2.2.2 and 6**). On average, the peats we examined have about 2.5 cable roots per cm of core, in contrast to peat-marls with 1 cable root every 5 cm of core. Pure fresh water marl exhibits no mangrove cable roots.

**Vertical distribution.** Profile TDWW is dominated by marl, which is replaced gradually by mangrove peat-marl, and eventually mangrove peat at the very top (**Figure 2.2.2**). TDE is peat-marl which gradually becomes mangrove peat at  $\sim 16$  cm depth. TF is mangrove peat. The trend in the interior, beyond a few hundred meters from the coast, is for basal marl to be gradually replaced by mangrove peat-marl and then peat. This is a response to increased sea level causing salt water encroachment and transport of mangrove propagules.

**Horizontal distribution.** At the present surface mangrove peat is found along the coast and is replaced landward by mangrove peat-marl and further inland, to a lesser extent, by patchy marl sediments.

**Interpretation problems.** Amorphous OC is the component that washes thru the fine sieve and retains few recognizable fragments. Amorphous material is either the product of decomposition of higher plants or is derived from the periphyton mat. No attempts were made to differentiate

between the two, although amorphous OC is more abundant in marls that contain sawgrass material. Most sawgrass communities in the Southeast Saline Everglades (SESE) contain well developed periphyton mats. The reason why periphyton mats without sawgrass contain less amorphous material may be due to decomposition, although this is not documented. At this time, then, the amorphous carries less paleoecological information than the larger OC fragments.

**Trends in sediment distribution.** The TDE core is composed of marl in the lower section, increasing in mangrove organic material until sediment interval 15-16 cm, where mangrove peat is observed, then continuing to the present land surface (**Figure 2.2.6**). At the accretion rate of 3.2 mm yr<sup>-1</sup>, equivalent to 3.1 yr cm<sup>-1</sup>, mangrove peat has been accreting at this location for ~ 51 yr, or since 1965 (Meeder et al. 1996). This is especially interesting as the construction of the L31E, which interrupted fresh water flow to Biscayne Bay, occurred very close to this date (Meeder et al. 1996). The salinity peak dates back to 1983 but is very likely to be 1993 (Hurricane Andrew), as most mollusks in this section are broken, eroded, discolored, leached and mixed with fresh water mollusks, evidence of marine mollusk transport. The transition from marl to peat occurred over a 20 cm interval, or between 64 and 167 years depending upon accretion rate.

In both interior cores, i.e., TDWW (25 m east of levee) and TDE (400 m east of the levee), sediments were marl with minor amounts of sawgrass organic material at the base changing upwards into mangrove peat-marl and mangrove peat at the top (**Figure 2.2.2**). The difference between TDWW and TDE is the thickness of the surficial mangrove peat, which is only 2-3 cm thick at TDWW and 16cm at TDE. This landward thinning is the result of transgressive seas causing salt water encroachment and mangrove propagule ingress; the furthest inland location has had less time for mangrove peat development.

The TF core was composed entirely of red mangrove peat deposited under marine conditions (**Figure 2.2.8**).

### **Trends in sediment salinity.**

**Vertical.** Salinity based upon the calculated SI increased upward in both TDWW and TDE from fresh water to marine influenced, while the sediment profile from TF was entirely marine influenced.

**Horizontal.** The thickness of the marine influenced sediment package decreased landward. This is because the length of time the surface was subjected to marine waters decreases landward, a result of increasing salt water encroachment associated with sea level rise.

**Paleoecology.** The mollusk assemblage changes not only in species composition but in mode of living. The freshwater mollusk assemblage is dominated by macro-phytophagous algal-diatom scraping epifauna. The marine sediments are characterized by filter feeders with macro-phytophagous feeding animals second in abundance, and arboreal species. The filter feeders are most abundant where frequent tidal flooding carries particulate material. In conclusion, the soil cores document salt water encroachment and a shift from fresh water marl deposition to salt tolerant mangrove peat.

**Stratigraphy.** The stratigraphy of the Mowry Canal transect displays a transgressive sequence, i.e., marine sediments overlying fresh water sediments, which thin landward. Sediment type is strongly associated with salinity index, sawgrass peat-marl is typical of fresh water plant communities, marl is transitional and mangrove peat is marine. Sediment type is therefore also strongly associated with plant community, sawgrass producing marl-peat sediments via a periphyton community, and marl and peat with mangroves.

### ***Summary***

1. Peats are composed of below ground biomass, with very little evidence of compaction.
2. A transgressive stratigraphic sequence is identified as mangrove peat expands or retreats landward over fresh water marl sediments in response to rising sea level.
3. The peat contains considerably more OC than the marl. Therefore, the OC storage capacity increases with salt water encroachment in marl environments.

### **3. Soils**

#### **3.1. Root biomass**

### ***Introduction***

Large volumes of organic carbon are stored in root biomass. In coastal wetlands, plants often have as much or more biomass belowground as above (Krauss 2013). The storage of biomass belowground also increases soil elevation by increasing soil volume (McKee et al. 2007). Therefore understanding how belowground biomass changes across an ecotonal gradient is essential for predicting changes and conserving valuable coastal wetlands. The “white zone” of the Florida Everglades is shifting inward as sea levels rise and salinity intrudes into brackish and freshwater marsh, altering both the biotic and abiotic structure of the ecosystem. Mangroves are encroaching inland, strongly altering the biotic structure of the environment while salinity and phosphorus levels increase with encroaching seawater. Abiotic and biotic shifts will likely alter belowground biomass storage and may influence climate change globally and wetland vulnerability locally.

### ***Methods***

We measured root biomass with a PVC coring device (5 cm diameter, 30 cm depth) in three vegetation plots (the most northern, southern and central plot) at each site (n=65). Samples were transported to the lab, kept below 5° C until processing. Samples were then rinsed over a 1 mm sieve, and live roots were separated based on buoyancy, texture and color. Roots were then dried to constant weight and weighed.

We compared site level average root biomass to site level vegetation structure (percent mangrove cover) and site distance from coast. Additionally, we regressed individual root samples against vegetation cover at the 1 m<sup>2</sup> plot level.

## Results

Site average root biomass is reported in **Table 3.1.1**. Site average root biomass decreased exponentially with site distance from coast (**Figure 3.1.1**), and increased exponentially as *R. mangle* cover increased (**Figure 3.1.2**). Vegetation cover on the 1 m<sup>2</sup> scale was not related to local root biomass (**Figure 3.1.3**).

**Table 3.1.1:** Mean and standard deviation of root biomass from 3 (5 cm diameter, 30 cm deep) cores per site.

Site	Mean Root biomass (g m <sup>2</sup> )	SD
CDW	1175.65	142
EP12R	472.35	554.02
EVER1	216.55	138.16
M5-N	44.86	17.19
TA2.2	127.19	96.91
TA2.3	140.68	111.26
TA2.4	785.68	368.63
TA2.5	214.24	114.55
TA2.6	414.36	187.26
TA3.3	443.48	220.98
TA3.5	161.28	79.55
TANGLN	219.35	124.38
TANGLIN	470.02	486.00
TANGLS	519.53	492.79
TDE	752.05	337.2
TDW	1746.56	136.23
TKYE	434.57	92.24
TKYINT	261.39	115.12
TKYNW	130.10	55.11
TKYW	434.22	260.56
UHC	427.25	145.83
UJB	180.13	77.94

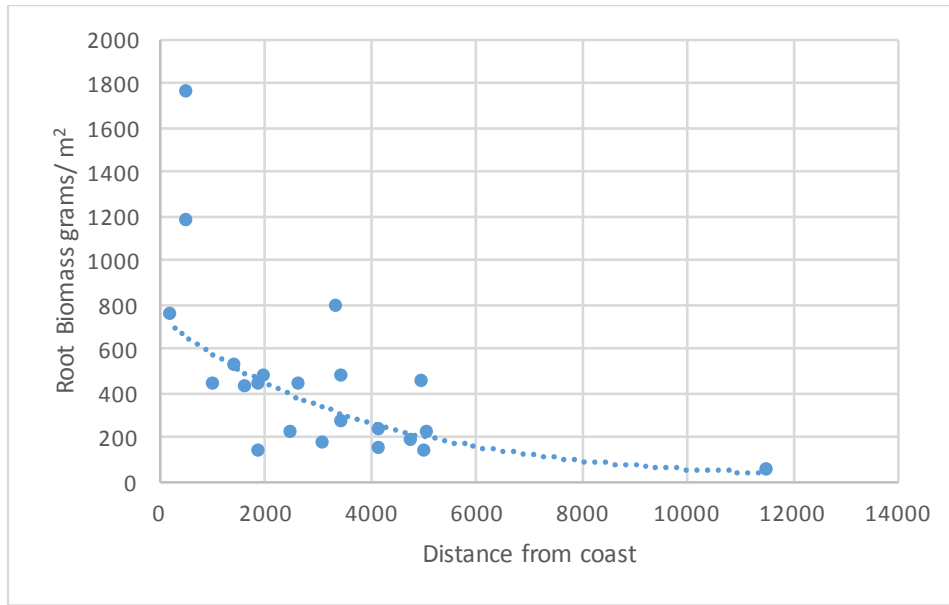


**Figure 3.1.1:** Average belowground root biomass (0-30 cm) related negatively and exponentially to distance from coast (Adjusted  $R^2=0.55$ ;  $P<0.001$ ). We determined percent mangrove cover in 30 1 m<sup>2</sup> plots along the perimeter of the circle.

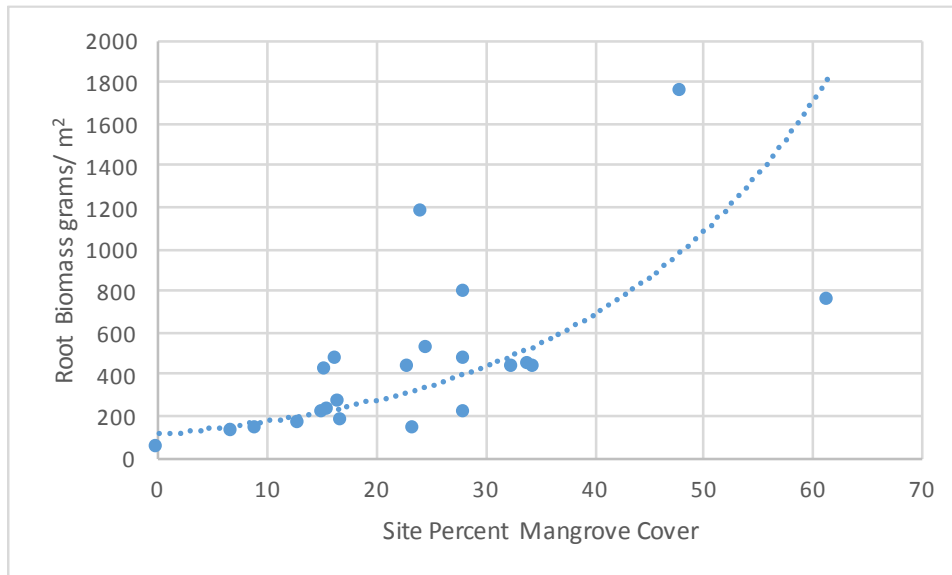


**Figure 3.1.2:** Average belowground root biomass (0-30 cm) related exponentially to site (a circle with 50 m radius) percent mangrove cover (Adjusted  $R^2=0.53$ ;  $P<0.001$ ). We determined percent mangrove cover in 30 1 m<sup>2</sup> plots along the perimeter of the circle.

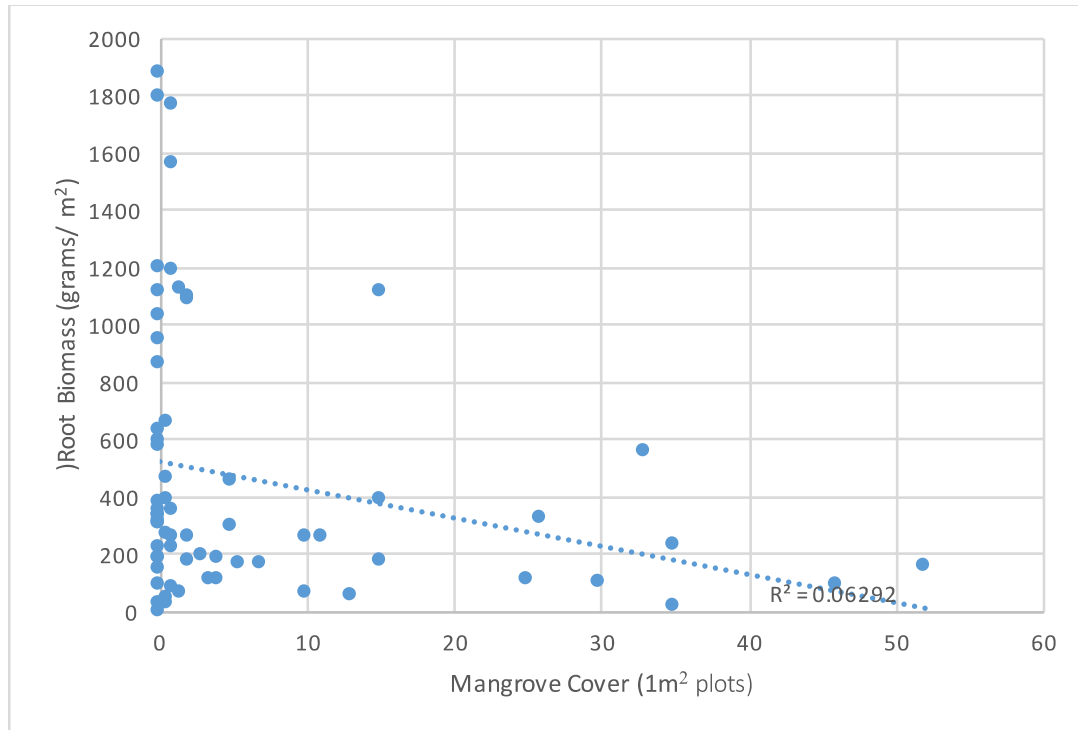


**Figure 3.1.3:** Relationship between root biomass and mangrove cover within their 1 m<sup>2</sup> plots ( $R^2=0.06$ ;  $P>0.05$ ).

### ***Discussion***

Root biomass is related to both mangrove cover and inversely to distance from coast. Our findings suggest that as mangroves encroach into marsh systems along a coastal wetland ecotone, root biomass increases. The exponential nature of the relationship between root biomass and vegetation transition indicates either a) potential interaction between cover and abiotic conditions associated with distance to coast b) amplification of the impact of root biomass based on ecosystem development or c) a combination of the two.

Our results show that vegetation structure at the one m<sup>2</sup> scale is not related to root biomass. Perhaps 1 m<sup>2</sup> is too small of a scale to influence root biomass. Mangrove roots in particular are known to extend many meters from the tree, particularly in the dwarf and shrub mangroves in our study sites.

The accumulation of root biomass can lead to the sequestration of organic carbon and increased sediment elevation. Roots often represent the most important component of carbon storage in coastal wetlands (Krauss 2013) because of their recalcitrant nature and storage in anaerobic soil (Middleton and McKee 2001), often persisting for thousands of years and driving sediment elevation increases (McKee et al. 2007).

Alternatively, vegetation shifts to species with higher root mass may alter root priming and potentially release stored organic matter, causing wetlands to lose elevation (Kuzyakov et al. 2010; Bernal et al. 2016). A loss of existing organic carbon may have particular impact with mangrove encroachment, due to high rates of rhizosphere oxidation (Gill and Tomlinson 1977; Scholander et al. 1995).

Currently we are measuring belowground productivity and breakdown rates adjacent to the location of our root biomass measures. We plan to use belowground productivity to determine how shifting vegetation impacts flux rates of organic carbon from coastal wetland soils.

### 3.2. Soils

Surface soils (to about 40 cm depth) were collected at the centers of the 24 plots (**Figure 2.1.1**). Once returned to the lab, soil profiles were described and the chemical and physical properties of each visible stratum are currently being analyzed separately. The following soil parameters are being determined: fresh bulk density, pH, water content, ash content, ash-free dry mass, total nitrogen, total carbon, total phosphorus, water soluble P, bicarbonate-soluble P. Plans to include analyses of soil enzyme activity had to be delayed due to logistical difficulties. Analyses of soil properties are currently being collated and interpreted, and will be presented in detail in the 2017 Annual Report.

### OTHER PRODUCTS

Scientists working on the project presented papers at two meetings during the summer of 2016. We made three presentations at the 4<sup>th</sup> Annual Mangroves and Macrobenthos (MMM4) meeting in St. Augustine, July 18-22, 2016 based on our previous work in the C111 study area. Mike Ross made an oral presentation “Disturbance, site and vegetation feedbacks create landscape structure in South Florida coastal wetlands”. Danielle Ogurcak also discussed “The detection of disturbance in the Southeast Saline Everglades, and its relationship to mangrove forest transgression”. Finally, Jack Meeder presented a poster on the important topic of “Saltwater encroachment and prediction of ecosystem response to the Anthropocene Marine Transgression, Southeast Saline Everglades, Florida”. At the Ecological Society of America’s 101<sup>st</sup> Annual Meeting (Ft. Lauderdale, FL; August 7-12, 2016), Mike Ross organized a session on “Ecosystems in motion: thresholds of resilience to the press disturbances of sea level change among North American coastal landscapes”. At that session, Jack Meeder’s talk, “The threshold rate of sea level rise determining resilience vs. non-resilience in southeast Florida coastal wetlands”, was based largely on data from the study area. In October, 2016, the following paper was submitted for review in *Hydrobiologia*: “Coastal response to the Anthropocene marine Transgression, Southeast Saline Everglades” by J. F. Meeder, R. Parkinson, P.W. Harlem, P. Ruiz and M.S. Ross.

Three FIU graduate students began working on the C-111 project this year. Rosario Vidales, who began her doctoral program in the Department of Earth and Environment during the Fall 2016 semester, will work on the relationships of vegetation, soil and water in the very dynamic coastal landscape. Rosario has already contributed greatly in the field, in sample processing, and in data analysis highlighted in Section 1.3. Himadri Biswas, who is beginning his doctoral program in E&E in January, will be addressing some of the same landscape processes, using remote sensing as his primary tool. Sean Charles is in the fourth year of his program in the Department of Biological Sciences. His dissertation work focuses on the impacts of mangrove invasion into coastal marshes at the ecosystem scale. His work plan includes the study of root production in wetlands east of Taylor Slough, and preliminary results are reported in Section 3.1.

Our work has also benefitted from the help of a high school student, Katarzyna Bezen who processed five sediment cores (TKYE, TKYINT, TKYNW, TKYW and TANGLS) for the content and different types of organic material. In addition, she will present the results of her investigation at Miami Dade Science Fair in Miami, Junior Science, Engineering and Humanities Symposium at University of Florida in Gainesville and FCE-LTER meeting in Miami in the upcoming few months. She will present these results in addition to diatom analysis of few samples from one of the cores mentioned above that, she is currently analyzing.

#### PLANS FOR 2016-17

Our plan for 2017 is to complete most of the remaining fieldwork, leaving 2018 to spend more time on data analysis and publication of summary papers. In 2017, we plan to complete the marsh sampling. Some tree island work will likely remain, but since December 2016, we have already sampled 13 tree islands (not reported on here). During these trips, we have observed large changes since our earlier (1995) survey, with the invasion of red mangrove into the forest understories the most evident. In 2017, we will also begin determination of sediment accretion rates through Pb-210 dating, relating these rates to the sediment types. Jack Meeder, Mike Ross, and Rosario Vidales all plan to present project data at the Society of Wetland Science Annual Meeting in San Juan, P.R., in June 2017.

#### LITERATURE

- Castañeda-Moya, E., Twilley, R. R., & Rivera-Monroy, V. H. (2013). Allocation of biomass and net primary productivity of mangrove forests along environmental gradients in the Florida Coastal Everglades, USA. *Forest Ecology and Management*, 226-241.
- Clarke, KR, Warwick RM (2001). Change in marine communities: an approach to statistical analysis and interpretation, 2nd edition. PRIMER-E, Plymouth, 172pp.
- DeVries, Ben, Jan Verbesselt, Lammert Kooistra, and Martin Herold. 2015. "Robust Monitoring of Small-Scale Forest Disturbances in a Tropical Montane Forest Using Landsat Time Series." *Remote Sensing of Environment* 161: 107–121
- Gaiser, E.E., Wachnicka, A., Ruiz, P., Tobias, F.A., Ross, M.S., 2005. Diatom indicators of ecosystem change in coastal wetlands. In: Bortone S. (Ed.), *Estuarine Indicators*. CRC Press, Boca Raton, FL, pp. 127-144.
- Masek, J.G., Vermote, E.F., Saleous N.E., Wolfe, R., Hall, F.G., Huemmrich, K.F., Gao, F., Kutler, J., and Lim, T-K. 2006. A Landsat surface reflectance dataset for North America, 1990–2000. *IEEE Geoscience and Remote Sensing Letters* 3(1):68-72.
- McCune and Grace 2002. McCune, B. and M. J. Mefford. 2011. PC-ORD. Multivariate Analysis of Ecological Data. Version 6.0. MjM Software, Gleneden Beach, Oregon, U.S.A.
- Meeder, J.F., M.S. Ross, G.T. Telesnicki, P.L. Ruiz and J.P. Sah. 1996. Vegetation analysis in the C-111-Taylor Slough Basin. Document 1. The Southeast Saline Everglades revisited a half-century of coastal vegetation change, 56p. Document 2. Marine transgression in the

- Southeast Saline Everglades, Florida; rates, causes and plant-sediment responses. 95p. Final report to the SFWMD.
- Powell, M. D., and S. H. Houston. 1996. Hurricane Andrew's landfall in south Florida. Part II: Surface wind fields and potential real-time applications. *Weather and Forecasting* 11:329–349.
- Ross, M. S., Meeder, J. F., Sah, J. P., Ruiz, P. L., and Telesnicki, G. J. 2000. The southeast saline Everglades revisited: 50 years of coastal vegetation change. *Journal of Vegetation Science*, 11(1), 101-112.
- Ross, M. S., Ruiz, P. L., Telesnicki, G. J., and Meeder, J. F. 2001. Estimating above-ground biomass and production in mangrove communities of Biscayne National Park, Florida (USA). *Wetlands Ecology and Management*, 9(1), 27-37.
- Smith III, T. J., & Whelan, K. R. (2006). Development of allometric relations for three mangrove species in South Florida for use in the Greater Everglades Ecosystem restoration. *Wetlands Ecology and Management*, 409-419.
- Verbesselt, J., A. Zeileis, and M. Herold. 2012. "Near Real-Time Disturbance Detection Using Satellite Image Time Series." *Remote Sensing of Environment* 123: 98–108.
- Wachnicka, A., Gaiser, E., Collins, L., Frankovich, T. and Boyer, J. 2010. Distribution of diatoms and development of diatom-based models for inferring salinity and nutrient concentrations in Florida Bay and adjacent coastal wetlands (U.S.A.). *Estuaries and Coasts*, 33(5):1080-1098.
- Wachnicka, A., Gaiser, E., and Boyer, J. 2011. Autecology and distribution of diatoms in Biscayne Bay, Florida: Implications for bioassessment and paleoenvironmental studies. *Ecological Indicators*, 11(2):622-632.
- Wachnicka, A., Gaiser, E., Wingard, L., Briceño, H., and Harlem, P. 2013a. Impact of the late Holocene climate variability and anthropogenic activities on Biscayne Bay (Florida, U.S.A.) environment: evidence from diatoms. *Palaeogeography, Palaeoclimatology, Palaeoecology* 371: 80-92.
- Wachnicka, A., Collins L., and Gaiser, E. 2013b. Response of diatom assemblages to 130 years of environmental Change in Florida Bay (U.S.A.). *Journal of Paleolimnology* 49(1): 83-101.
- Wachnicka, A., Gaiser, E., and Collins, L. 2013c. Correspondence of historic salinity fluctuations in Florida Bay, U.S.A., to atmospheric variability and anthropogenic Changes. *Journal of Paleolimnology* 49 (1): 103-115.
- Wachnicka, A., and Wingard, L. 2015. Biological indicators of changes in water quality and habitats of the coastal and estuarine areas of the Greater Everglades ecosystem. In: *Microbiology of the Everglades ecosystem* (Eds. Entry, J., Jayajandrachan, Gottlieb, A., and A. Ogdam). Science Publisher, pp. 218-240.

Zhang, K., B. Thapa, M. Ross, and D. Gann. 2016. Remote sensing of seasonal changes and disturbances in mangrove forest: a case study from South Florida. *Ecosphere* 7(6):e01366.